Med Chem Res
DOI 10.1007/s00044-016-1517-y

MEDICINAL CHEMISTRY RESEARCH

ORIGINAL RESEARCH

# Design and development of pyrrole carbaldehyde: an effective pharmacophore for enoyl-ACP reductase

**Shrinivas D. Joshi[1] · Devendra Kumar[1] · Uttam A. More[1] · Kap Seung Yang[2] · Tejraj M. Aminabhavi[1]**

Received: 18 March 2014 / Accepted: 25 January 2016


**Abstract** Enoyl-ACP reductase is the key enzyme involved in FAS-II synthesis of mycolic acid in bacterial cell wall and is a promising target for discovering new chemical entity. The designed pharmacophores are the possible better tools to combat mutation in enoyl-ACP enzyme, which leads to a decrease in volume of triclosan binding site. Compound **3a** showed H-bonding interactions similar to that of triclosan with enoyl-ACP enzyme and with a better docking score (C score 8.81), while the compound **3f** showed additional interaction with MET98.H amino acid residue. The 3D-QSAR computations also support the docking study to develop novel pyrrole-based derivatives.

*Graphical abstract* Molecular docking 3D-QSAR studies and synthesis of active analogs of pyrrole carbaldehyde as better receptor fit pharmacophore for enoyl-ACP reductase along with in vitro antitubercular activity.

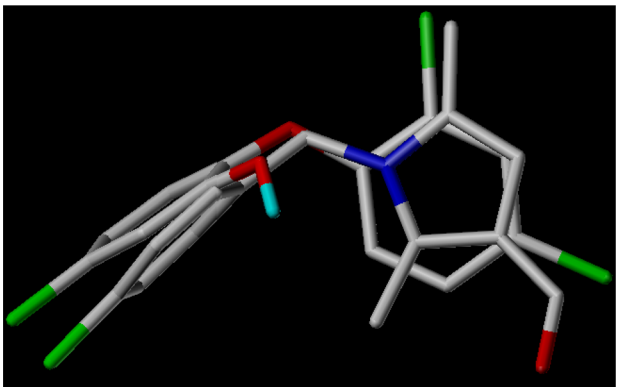

**Keywords** Pyrroles · Antitubercular activity · Molecular docking · 3D-QSAR · Enoyl-ACP reductase

## Introduction

Tuberculosis (TB) is a leading cause of death worldwide, despite the global efforts and financial investment by the government and non-governmental organizations in disease control (Raviglione *et al.*, 2012). According to WHO 2012 global report on TB, it was estimated that 3.7 % (range 2.1–5.2 %) of new cases and 20 % (range 13–26 %) of the previously treated cases have multidrug-resistant tuberculosis (MDR-TB). In Eastern Europe and Central Asia, 9–32 % of the new patients and more than 50 % of the previously treated patients are affected with MDR-TB (WHO, Global Report, 2012). Such global increase in the resistance of MDR-TB reflects inappropriate use of anti-TB drugs during the treatment course of patients with drug-susceptible strains (Espinal *et al.*, 2001). Additional factors like immigration, sex, age, HIV infection and

**Electronic supplementary material** The online version of this article (doi:10.1007/s00044-016-1517-y) contains supplementary material, which is available to authorized users.

✉ Shrinivas D. Joshi
shrinivasdj@rediffmail.com

Kap Seung Yang
ksyang@chonnam.ac.kr

[1] Novel Drug Design and Discovery Laboratory, Department of Pharmaceutical Chemistry, S.E.T's College of Pharmacy, Sangolli Rayanna Nagar, Dharwad 580 002, India

[2] Department of Polymer and Fiber System Engineering, Chonnam National University, 300 Yongbong-Dong, Bukgu, Gwangju 500 757, Korea

Published online: 09 February 2016

socioeconomic factors have shown to be associated with the increased prevalence of MDR-TB (Faustini *et al.*, 2006). Almost half of the global MDR-TB cases have been reported from the heavily populated areas of China and India (WHO, Global Report, 2010).

Isoniazid (INH), a frontline antitubercular agent, is a pro-drug that requires activation to form the active metabolite (INH-NAD adduct), which exerts its lethal effect on intracellular target (Zhang *et al.*, 1992; Johnsson and Schultz, 1994; Johnsson *et al.*, 1995). The INH-NAD adduct inhibits mycolic acid biosynthesis in *Mycobacterium tuberculosis* by affecting the InhA, an enoyl-ACP reductase enzyme of the type II fatty acid synthesis (FAS-II) system, which catalyzes the last step of fatty acid elongation cycle (Quemard *et al.*, 1991). Among these, fatty acid biosynthesis-I (FabI) constitutes a single isoform in the majority of pathogens such as *Staphylococcus aureus* (Heath *et al.*, 2000), *Escherichia coli* (Heath and Rock, 1995) and *M. tuberculosis* (Banerjee *et al.*, 1994). The clinical success of InhA inhibitor INH (Quemard *et al.*, 1995) and numerous reports of FabI inhibitors (Lu and Tonge, 2008) involving the diazaborines (Baldock *et al.*, 1996), 4-pyridones (Kitagawa *et al.*, 2007), naphthyridinones (Seefeld *et al.*, 2003), triclosan and analogs (McMurry *et al.*, 1998; Chhibber *et al.*, 2006; Park *et al.*, 2007; Sivaraman *et al.*, 2004; Sullivan *et al.*, 2006; Tipparaju *et al.*, 2008) have validated this target as one of the most attractive of the FASII pathway. This enzyme is recognized and validated as an important drug target in *M. tuberculosis*, since its homolog in the humans is absent.

Several azole compounds containing imidazole, pyrrole, and toluidine or methanamine group were tested for antimyobactrial activity against drug-resistant and intramacrophagic mycobacteria (Biava *et al.*, 1997; Fioravanti *et al.*, 1997). Among these, pyrrole derivatives BM212 seem to be endowed with potent and selective antimycobacterial properties (Deidda *et al.*, 1998). Recently, spontaneous mutants resistant to BM212 and SQ109 compounds with anti-TB activities have shown to contain mutations mapping to *mmpL3* (for mycobacterium large membrane protein) (La Rosa *et al.*, 2012). The *mmpL3* was found to be essential in mycobacteria and conditional depletion of *mmpL3* in *Mycobacterium smegmatis* that resulted in the loss of cell wall mycolylation (Varela *et al.*, 2012).

Of late, due to the availability of computational methods including 3D-QSAR tools like CoMFA and CoMSIA are being increasingly employed in rational drug discovery to understand the drug–receptor interactions for designing new molecules. In our previous work, we have reported the pyrrole analogs as antimycobacterial, antifungal and antibacterial agents (Joshi *et al.*, 2008, 2013a) on which docking 3D- and 2D-QSAR studies were performed (Joshi *et al.*, 2013b, 2014a, b; More *et al.*, 2014). Continuing our study on enoyl-ACP reductase, herein we report docking and 3D-QSAR studies of the newly synthesized compounds having antitubercular activity. The drug design concept of this study is based on the reported data of marketed drug containing pyrrole core (Aloracetam), developed by Aventis for the treatment of neurodegenerative disease (Fischer *et al.*, 2004) as well as the well-known antibacterial agent triclosan along with antimycobacterial agent BM212 (see Fig. 1).

## Molecular modeling/docking studies

The 3D structures were generated using the Chem draw 3D software. By using the standard bond lengths and bond angles, the geometry optimization was carried out with the help of standard Tripos force field (Clark *et al.*, 1989) with a distance-dependent dielectric function, energy gradient of 0.001 kcal/mol and Gasteiger–Huckel as the electrostatics. Conformational analyses of 23 compounds were performed using repeated molecular dynamics-based simulated annealing approach as implemented in Sybyl-X 2.0 (Tripos Inc., St. Louis, USA). All the conformations were minimized with Gasteiger–Huckel charges.

### Data set and structures

The in vitro antitubercular activity (expressed as minimum inhibitory concentration, MIC) was converted into pMIC (log MIC) values, which were used to construct the 3D-QSAR models. Structures and biological activities of the compounds are summarized in Table 1. The 3D-QSAR models were generated using a training set of 18 molecules; the predictive power of the resulting models was evaluated using a test set of five molecules. Test compounds were selected randomly such that the data set included diverse structures and a wide range of activity (diversity method).

### Alignment rule

A common substructure-based alignment was adopted, wherein molecules were aligned to the template molecule on a common backbone as illustrated in Fig. 2. For database alignment of the inhibitors, the structure of compound **3a** (bioactive conformation of the compound **3a**) was used.

### CoMFA and CoMSIA settings

In order to better understand and explore the contributions of electrostatic and steric fields in the binding affinity and potency of pyrrole scaffold as well as to build the

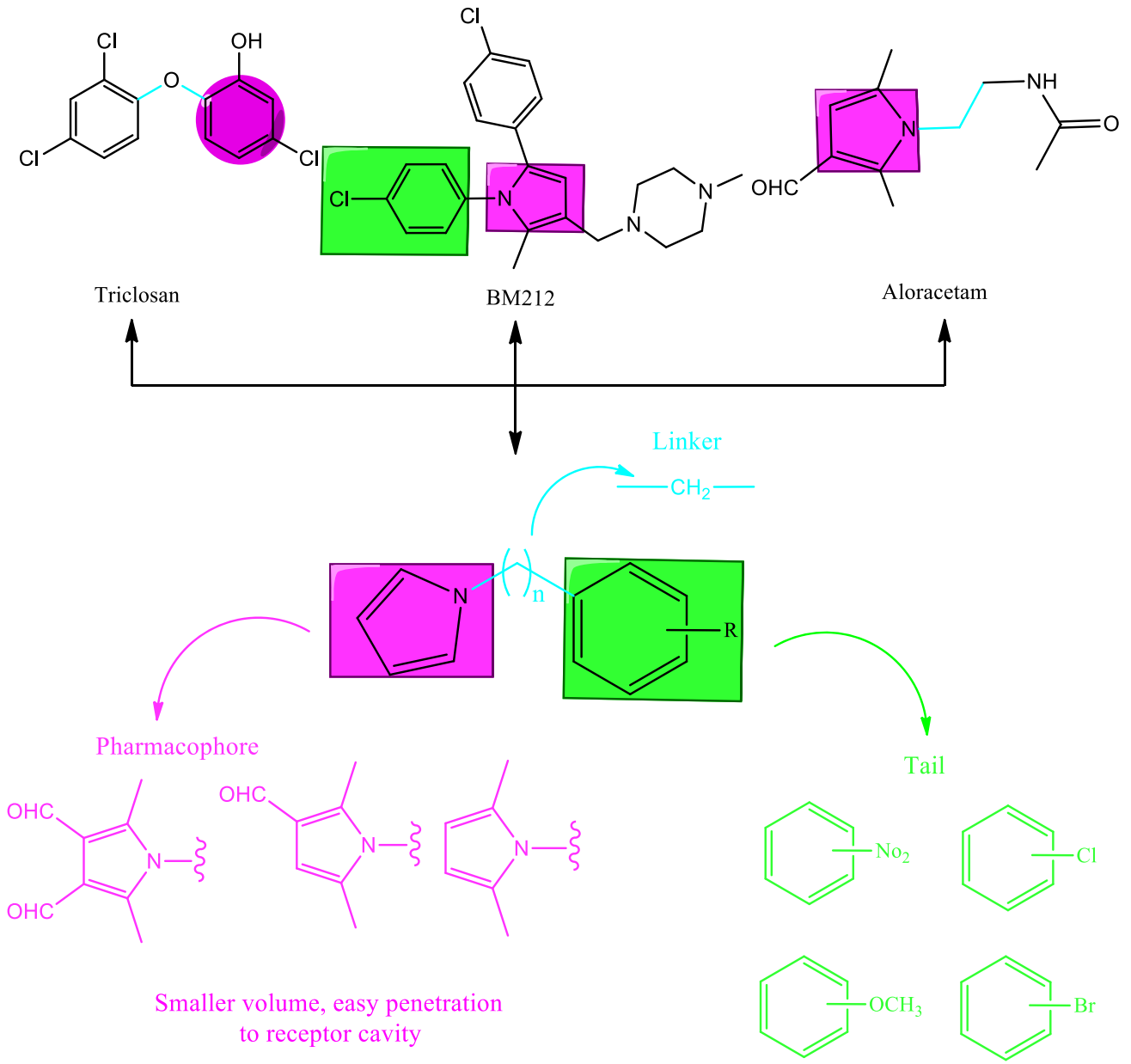


**Fig. 1** Searching for better receptor fit ligand in comparison with triclosan in enoyl-ACP receptor

predictive 3D-QSAR models, the CoMFA studies were performed based on molecular alignment. The contributions of steric and electrostatic fields were calculated using the Lennard–Jones and Coulombic potentials, respectively (Cramer *et al.*, 1989). The aligned training set of molecules was then placed in a 3D grid box to include the entire set. The CoMFA steric and electrostatic fields were generated at each grid point with Tripos force field using $sp^3$ carbon atom probe carrying $(a + 1)$ net charge.

The CoMFA grid spacing of 2.0 Å in $x$, $y$ and $z$ directions and the grid regions were generated by the CoMFA routine to encompass all the molecules with an extension of 2.0 Å in each direction. The CoMFA region focusing method was applied to increase the resolution of CoMFA models. The default value of 30 kcal/mol was the maximum steric and electrostatic energy cutoff. The CoMSIA was used in which similarity indices were calculated at different points on a regularly spaced grid for pre-aligned molecules. In this approach, four different similarity fields, viz, steric, electrostatic, hydrophobic and H-bond acceptor, were selected to cover major contributions to the ligand binding. In CoMSIA fields, singularities were avoided at atomic positions because the Gaussian type distance dependence of each physicochemical property was

**Table 1** Data set of chemical structures and their antitubercular activity against *Mycobacterium tuberculosis* $H_{37}Rv$ (**3a–w** and **2a**)

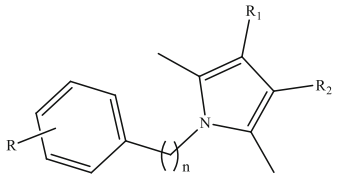


3(a-w), 2a

| Comp. no. | *n* | *R* | $R_1$ | $R_2$ | MIC (μg/ml) |
|---|---|---|---|---|---|
| **3a** | 0 | $3NO_2$ | H | CHO | 3.12 |
| **3b** | 0 | $4NO_2$ | H | CHO | 3.12 |
| **3c** | 0 | 4Cl | H | CHO | 6.25 |
| **3d** | 0 | 3Cl | H | CHO | 6.25 |
| **3e** | 0 | 4Br | H | CHO | 6.25 |
| **3f** | 0 | $2NO_2$ | H | CHO | 6.25 |
| **3g** | 0 | $4OCH_3$ | H | CHO | 25.0 |
| **3h** | 0 | 3Br | H | CHO | 12.5 |
| **3i** | 0 | 2Br | H | CHO | 25.0 |
| **3j** | 1 | 4Cl | H | CHO | 6.25 |
| **3k** | 1 | 3Cl | H | CHO | 3.12 |
| **3l** | 0 | $3NO_2$ | CHO | CHO | 6.25 |
| **3m** | 0 | $4NO_2$ | CHO | CHO | 6.25 |
| **3n** | 0 | 4Cl | CHO | CHO | 12.5 |
| **3o** | 0 | 3Cl | CHO | CHO | 12.5 |
| **3p** | 0 | 4Br | CHO | CHO | 12.5 |
| **3q** | 0 | $2NO_2$ | CHO | CHO | 6.25 |
| **3r** | 0 | $4OCH_3$ | CHO | CHO | 50.0 |
| **3s** | 1 | 4Cl | CHO | CHO | 6.25 |
| **3t** | 1 | 2Cl | CHO | CHO | 12.5 |
| **3u** | 0 | $3OCH_3$ | H | CHO | 25.0 |
| **3v** | 0 | 3Br | CHO | CHO | 12.5 |
| **3w** | 0 | 2Br | CHO | CHO | 25.0 |
| **2a** | 0 | $3NO_2$ | H | H | 6.25 |

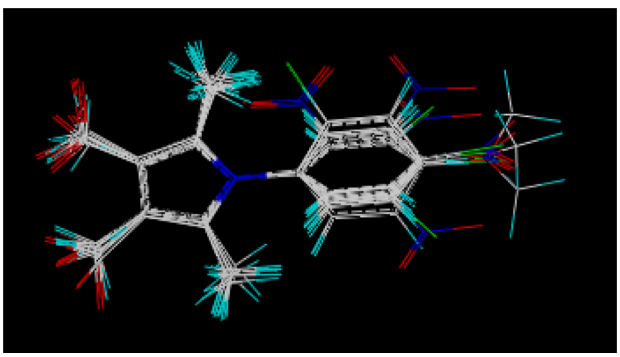

**Fig. 2** Database alignment against most active confirmation of compound **3a**

adopted, and thus, no arbitrary cutoffs were necessary, and default value of 0.3 was used as the attenuation factor (α).

## Partial least squares (PLS)

Partial least squares regression (PLS regression) is a statistical method that bears some relationship to the principal components regression; instead of finding hyperplanes of minimum variance between the response and the independent variables, it finds a linear regression model by projecting the predicted variables as well as the observable variables to a new space. All the latent variable path

models in PLS consist of three sets of relationships: (a) the inner model, which specifies the relationship between latent variables (LVs), (b) the outer model, which specifies the relationship between LVs and their association observed or manifest variables (MVs), and (c) the weight relations upon which the case values for LVs can be estimated. Without loss of generality, it can be assumed that LVs and MVs are scaled to zero means and unit variance such that location parameter (i.e., constant parameter terms) can be eliminated (Chin, 1998).

### Inner model

The inner model depicts the relationship among the latent variables based on substantive theory,

$$\eta = \beta_0 + \beta\eta + \xi + \zeta \quad (1)$$

where $\eta$ represents the vector of endogenous latent variables, $\xi$ is a vector of the exogenous latent variables and $\zeta$ is the vector of residual variable (Chin, 1998).

### Outer model

The outer model defines how each block of indicators relates to its latent variable. The MVs are partitioned into non-overlapping blocks. For those blocks with reflective indicators, the relationship can be defined as:

$$x = \Lambda_x\xi + \varepsilon_x \quad (2)$$

$$y = \Lambda_y\eta + \varepsilon_y \quad (3)$$

where $x$ and $y$ are the MVs for exogenous and endogenous LVs, $\xi$ and $\eta$, respectively. The terms $\Lambda_x$ and $\Lambda_y$ are the loading matrices, representing the simple regression coefficients connecting the LV and their measures. The residuals for the measure $\varepsilon_x$ and $\varepsilon_y$ in turn can be interpreted as measurement error (Chin, 1998).

The optimal number of components was determined with samples-distance partial least squares (SAMPLS) (Bush and Nachbar, 1993) and cross-validation was carried out by the leave one out ($L_{OO}$) method. The model with an optimum number of components (highest $q^2$) and with the lowest standard error of prediction (SDEP) was considered for further analysis. Equal weights were assigned to steric and electrostatic fields by CoMFA_STD scaling option. To speed up the analysis and reduce the noise, columns with $\sigma$ value of <2.0 kcal/mol were filtered off to compute the conventional $r^2$ using the optimum number of components. To further assess the robustness and statistical confidence of the derived models, cross-validation and bootstrapping (Cramer *et al.*, 1988) analysis for 100 runs was performed. Statistical calculation was performed on each of these bootstrap samplings. Models with a cross-validation ($q^2$) value of >0.5 were sought, since at this value, the probability of chance correlation was <5 % (Clark *et al.*, 1990).

### Predictive ability of CoMFA and CoMSIA models ($r^2_{pred}$)

In assessing a PLS model, we start by looking at the $r^2$ for each dependant LV provided by PLS for the structural model. This is obtained because the case value of the LVs is determined by the weight relations. The change in $r^2$ can be explored to see whether the impact of particular independent LV on a dependent LV has substantive impact. Specifically, the effect size, $f^2$ can be calculated as (Chin, 1998):

$$f^2 = \frac{r^2_{\text{included}} - r^2_{\text{excluded}}}{1 - r^2_{\text{included}}} \quad (4)$$

The value of $r^2$ is a measure of % data that can be satisfactorily explained by the regression analysis (Thomas, 2007). The application of special multivariate statistical analysis such as PLS analysis and $L_{OO}$ cross-validation ensures statistical significance of the final CoMFA equation. The outcome of this procedure is a cross-validated correlation coefficient, $q^2$, which is calculated as:

$$q^2 = 1 - \frac{\sum (y_i - \hat{y}_i)^2}{\sum (y_i - \bar{y})^2} \quad (5)$$

where $y_i$, $\hat{y}_i$ and $\bar{y}$ are actual, estimated and averaged activities, respectively. However, the statistical meaning of $q^2$ is different from the conventional $r^2$ that is a $q^2$ value >0.3 is often considered significant (Agarwal *et al.*, 1993). By PLS analysis, $r^2$ predicted for CoMFA and CoMSIA were 0.81 and 0.56, respectively. Cross-validated and non-cross-validated statistical parameters of CoMFA and CoMSIA models are summarized in Table 2.

### Molecular docking and scoring

The protein coordinate of enoyl-ACP reductase from *M. tuberculosis* (2X22) bound to PT70 was downloaded from the Protein Data Bank (Luckner *et al.*, 2010). The ligand was separated from the protein, and hydrogens were added to free templates for protein residues. All the compounds were docked using Sybyl-X 2.0 software (Tripos Inc., St. Louis, USA). Compounds that were docked in this study contain Gasteiger–Huckel charge, while the biopolymer contains Amber7FF99 charges; the geometry of the enzyme was optimized using the Tripos molecular mechanics force field. Docking was carried on 2X22 (A chain) protein using the default setting of Sybyl-X 2.0 program, in which all the water molecules were removed

**Table 2** Statistical parameters of CoMFA and CoMSIA models by the PLS analysis

| Method | Parameters | CoMFA | CoMSIA |
|---|---|---|---|
| Cross-validation | Optimal components | 2 | 2 |
| | $r^2_{loo}$ | 0.81 | 0.56 |
| | $r^2_{pred}$ | 0.81 | 0.54 |
| | $r^2_{bs}$ | 0.87 | 0.73 |
| | $SD_{bs}$ | 0.02 | 0.05 |
| | $q^2$ | 0.58 | 0.53 |
| Non-cross-validation | $r^2$ | 0.86 | 0.72 |
| | SEE | 0.13 | 0.19 |
| | $F$ | 98.13 | 40.00 |

| PLS parameters | Norm coefficient | Fraction | Norm coefficient | Fraction |
|---|---|---|---|---|
| Steric | 0.74 | 0.28 | 0.13 | 0.17 |
| Electronic | 0.75 | 0.29 | 0.16 | 0.21 |
| H-bond donor | – | – | 0.01 | 0.12 |
| H-bond acceptor | – | – | 0.17 | 0.22 |

and essential H atoms were added randomly and then the Dock scores were evaluated by the consensus score (C score) (Clark *et al.*, 2002). The C score integrates a number of popular scoring functions for ranking the affinity of ligand bound to the active site of a receptor. The strengths of individual scoring functions combine to produce a consensus that is more robust and accurate than any single function for evaluating the ligand–receptor interactions. Moreover, the D score, PMF score (potential of mean force) (Muegge and Martin, 1999), G Score (Kuntz *et al.*, 1982) and Chem Score (Eldridge *et al.*, 1997) were also calculated to get better insights.

## Results and discussion

### Chemical synthesis

Compounds **2a**–**w** were synthesized (Scheme 1) using the well-known *Paal–Knorr* pyrrole synthesis with different substituted anilines **1a**–**w** and α,β-diacetyl compound (hexane-2,5-dione) in a polar protic solvent medium. Conversion of **2a**–**w** to different mono-substituted and di-substituted pyrrole carbaldehydes follows the Vilsmeier–Haack mechanism, which is the reaction between substituted amide and phosphrous–oxychloride along with an electron-rich arene to produce aryl aldehyde or ketone (Vilsmeier and Haack, 1927; Mallegol *et al.*, 2005). For formylation of aromatic compound, it is necessary to have electron donating group either by resonance or by inductive effect. Compounds **3a**–**w** were synthesized using $POCl_3$ and DMF in a solvent-free medium at 45–110 °C for 1–4 h to obtain improved yields of pure compounds.

All the compounds were purified by column chromatography and characterized by FTIR, $^1$H NMR, $^{13}$C NMR, mass spectrometry and elemental analysis. FTIR spectra of compounds suggest characteristic features of all the synthesized compounds (**3a**–**w**) that contained C=O stretching at 1648–1715 $cm^{-1}$ along with the stretching band due to Fermi-resonance around 2800–2850 and 2700–2750 $cm^{-1}$ due to aldehydic group. The $^1$H NMR and $^{13}$C NMR spectra showed a singlet around 9.5–10.2 and 164–185 ppm, respectively, further confirming the presence of aldehydic group. In addition, elemental

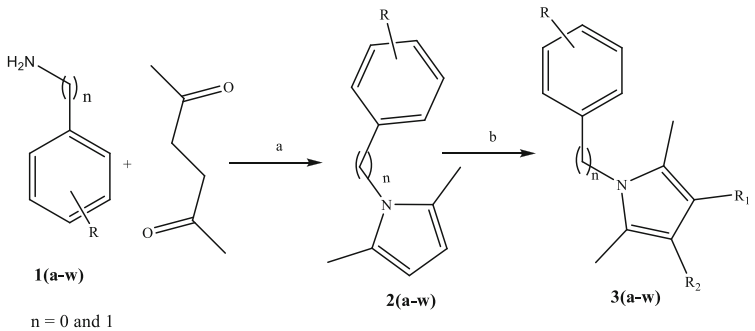


**Scheme 1** Synthesis of 2,5-dimethylsubstitutedphenyl/benzyl-1*H*-pyrrole-3/4-mono/dicarbaldehydes. Reagents and conditions: **a** acetic acid, reflux 110–120 °C, 30 min. **b** DMF, $POCl_3$, 2–4 h

analysis in conjunction with mass spectra confirmed the incorporation of aldehydic group at the 3rd and 4th positions of pyrrole with the major protonated molecular ion peak observed at their corresponding *m/z* value as assumed theoretically.

## Antitubercular activity

The MIC values of the compounds versus selected *M. tuberculosis* $H_{37}Rv$ are given in Table 1. Antitubercular activity was performed by Alamar Blue dye method (Franzblau *et al.*, 1998; Lourenco *et al.*, 2007); standard values for antitubercular tests were performed, and these values are: 3.125 (Pyrazinamide), 6.25 (Streptomycin) and 3.125 μg/ml (Ciprofloxacin). Compounds **3a**, **3b** and **3k** exhibited antitubercular activity at MIC of 3.12 μg/ml. Compounds **3a**, **3b** and **3k** inhibited the mycobacterium growth quite effectively compared to others in the series. These compounds are evolved to be the most active in the series investigated. MIC values of all other compounds are around 6.25–50 μg/ml.

## Molecular modeling

Earlier, we have reported on the molecular docking study of pyrrolyl hydrazones, using MMFF94 charges and found 6.18 C score for triclosan (TCL) (More *et al.*, 2014). In the present study, we have used Amber7FF99 for the biopolymer and Gasteiger–Huckel charges for small molecules to carry out the docking study; with this charge, TCL showed 6.01 C score, but retained its interaction with Tyr158 and cofactor $NAD^+$ was used as a standard drug to compare other molecules in the series. The synthesized compounds, **3a** and **3f**, occupy the same binding site as that of TCL (Fig. 3). Oxygen atom of $NO_2$ group at the *meta* position to benzene (compound **3a**) showed interaction with the hydrogen of Tyr158.OH amino acid as well as the interaction with cofactor NAD1270.H21. Oxygen atom of aldehydic group at the 3rd carbon of pyrrole (compound **3f**) showed interaction with MET68.H amino acid residue, but aldehydic group of compound **3a** did not show any interaction similar to that of compound **3f** (Figs. 3, 4).

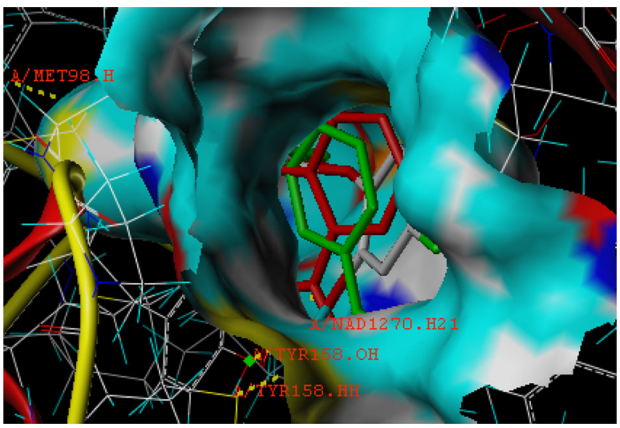


**Fig. 3** Docking poses of triclosan and highly active molecules **3a** (*green*) and **3f** (*red*) (Color figure online)

The C score that ranks the affinity of ligands bound to the active site of a receptor (Table 3) showed better affinity to compounds **3a, 3j, 2a, 3k, 3f** and **3e** (C score 8.81, 7.81, 7.70, 7.06, 6.87 and 6.40, respectively) than triclosan (C score 6.01). Only **3w** showed C score below 3 (C score 2.77) suggesting that the compounds in this study are the better hit molecules. Compound **3a** and triclosan showed the same pattern of interaction in the active site of the enzyme.

## CoMFA and CoMSIA models

Data sets of the newly synthesized pyrrole carbaldehydes were used to perform the 3D-QSAR studies, wherein all compounds were aligned to the most active conformation of compound **3a** (Fig. 2).

## Contour maps

The CoMFA contours map analysis for steric favored and disfavored regions are shown in Fig. 5a. The giant green contour map at the benzene ring showed increase in steric bulk with an increase in the activity. In case of electrostatic contour map (Fig. 5b) analysis, bunch of red counter near benzene showed the region favoring the negatively charged substituent. In case of CoMSIA analysis, the patterns of steric and electrostatic counter map are nearly identical (Fig. 6a, b) as observed in CoMFA. Due to these patterns of counter map of benzene, sterically favored electronegative substitution showed better MIC, CoMFA and CoMSIA pMIC values as shown in Tables 1 and 4 (compounds **3a**, **3b** and **3k** with the MIC of 3.12 μg/ml CoMFA Predicted = 5.6024, 5.5002, 5.4772 and CoMSIA Predicted = 5.5963, 5.5027, 5.4863, respectively). In both CoMFA and CoMSIA analysis, a yellow counter over the *ortho* position of benzene (Figs. 5a, 6a) is due to dwindling in the activity of compounds containing bulky substitution at this position (compounds **3f**, **3i**, **3q**, **3t** and **3w**). Both CoMFA and CoMSIA analysis confirmed our prediction that the size of a pharmacophore should be lesser (Figs. 5a, 6a). Bunch of yellow contour maps over the 3rd and 4th positions of pyrrole (Figs. 5a, 6a) defined the cause of hampering of activity in those compounds containing 2 aldehydic groups at the 3rd and 4th positions of pyrrole along with the electropositive substitution at the benzene ring (Figs. 5b, 6b) (compound **3r**, MIC 50 μg/ml).

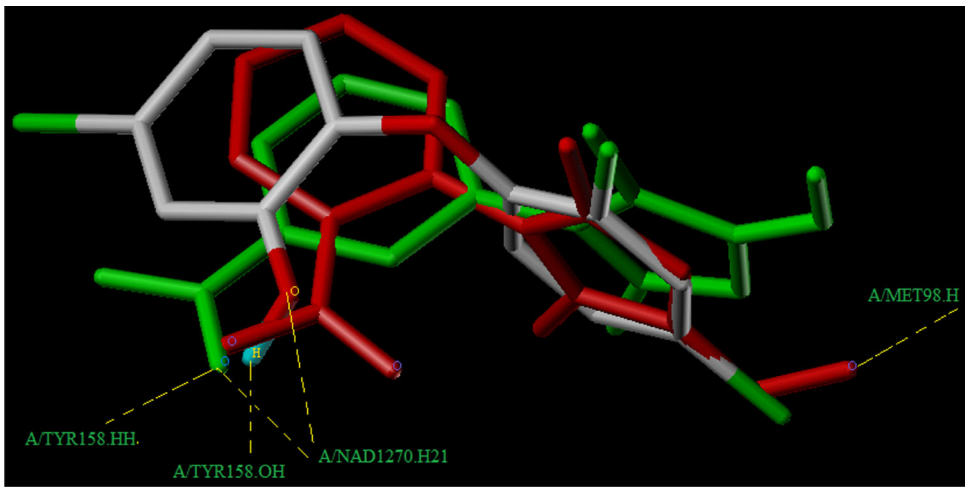


**Fig. 4** Docking poses of triclosan and highly active molecules **3a** (*green*) and **3f** (*red*) showing pattern of interaction (Color figure online)

The CoMSIA counter map analysis to understand the effect of hydrophobic and hydrophilic descriptors on the activity of compounds (Fig. 6c) suggested the linker to be hydrophilic in nature. In Fig. 6d, magenta contour over the 3rd and 4th positions of benzene and the same counter map over the 3rd position of pyrrole confirmed that H-bond acceptors at this position are favorable for the activity.

In both CoMFA and CoMSIA, a green contour map over the substituted benzene showed the requirement of steric bulk, favoring the activity (Figs. 5a, 6a). In the electrostatic field analysis (Fig. 5b), the electronegative group at the benzene ring has boosted the activity, but in case of **3a**, the nitro group is involved in H-bonding with Tyr158.HH (Fig. 4). Oxygen of aldehydic group at the 3rd position of pyrrole in **3f** exerts an interaction with Met 98.H amino acid residues. In CoMFA contour map analysis (Fig. 5a), steric bulk at the 3rd position of pyrrole showed strong interaction with the amino acid residue. Aldehydic group at the 3rd position of pyrrole is responsible for this additional interaction with the enzyme that would help to improve the anti-tuberculosis activity.

From the receptor-based drug designing (Figs. 3, 4) CoMFA (Fig. 5a) and CoMSIA (Fig. 6a), it can be concluded that aldehyde at the 3rd position of pyrrole is essential to increase the inhibitory potency of a drug and the MIC value of such aldehydic compounds (at the 3rd position of pyrrole) along with the electronegative substitution at the benzene ring fall in the range 3.12–6.25 μg/ml (except for compounds, **3g**, **3h** and **3i**). If we try to increase the number of aldehydic groups at the pyrrole 3rd and 4th positions to induce better interaction with the receptor pocket, but due to its unacceptable orientation and steric disfavoring region in the double aldehydic compounds, they lost their H-bonding interactions with Met 98. H (Figs. 5a, 6a) and the MIC values increased to 50 μg/ml, indicating that only one aldehydic group at the pyrrole moiety favors the activity.

In this work, main aim of our study is to develop those molecules that have better fit into the enoyl-ACP receptor. Crash score, which will be a sign of penetration of ligand to receptor cavity showed a comparable score of −1.98 for **3j** with triclosan (−2.08) and superior score of −2.62 for compound **3k**. On the basis of Crash score of **3k** as shown in Fig. 7, one can speculate that such hit molecules may easily get access to the active site of the enoyl-ACP reductase enzyme. Steric clash in between enoyl-ACP reductase enzyme cavity and triclosan due to the mutation of glycine 93 to valin would cause the resistance of triclosan to *E. coli* (Levy *et al.*, 1999). Such mutations in case of either *E. coli* or *M. tuberculosis* may be handled by the compounds evolved in this study.

## Experimental section

Melting points were determined using Shital-digital programmable apparatus and are uncorrected. FTIR spectra in KBr pellets were recorded on a Bruker FTIR spectrophotometer. The $^{1}$H and $^{13}$C NMR spectra were recorded on a Bruker AVANCE II at 400 and 100/75 MHz, respectively; chemical shifts are expressed in parts per million (ppm) relative to TMS. The abbreviations used to describe the peak patterns are: (b) broad, (s) singlet, (d) doublet, (t) triplet, (q) quartet and (m) multiplet. Some of the $^{13}$C NMR spectra were recorded at Chonnam National University, Gwangju, Korea (Courtesy of Prof. K. S. Yang).

Mass spectra (MS) were recorded in a JEOL GCMATE II GC-Mass spectrometer and Shimadzu QP 20105 GC-Mass spectrometer. Elemental analysis data (performed on

**Table 3** Docking score, C score, crash value, polar area and different scores of all studied compounds

| Comp. no. | C score[a] | Crash[b] | Polar[c] | D score[d] | PMF score[e] | G score[f] | Chem score[g] |
|---|---|---|---|---|---|---|---|
| **3a** (template) | 8.81 | 0.59 | 2.27 | −218.39 | −47.09 | −140.37 | −37.45 |
| **3j** | 7.81 | −1.98 | 0.00 | −198.46 | −32.66 | −167.38 | −32.10 |
| **2a** | 7.70 | −2.28 | 1.35 | −126.65 | −24.28 | −222.66 | −33.33 |
| **3k** | 7.06 | −2.62 | 0.00 | −236.39 | −22.89 | −273.94 | −34.48 |
| **3f** | 6.87 | −2.57 | 1.05 | −232.01 | −4.24 | −144.15 | −24.43 |
| **3e** | 6.40 | −2.62 | 0.01 | −136.51 | −22.89 | −217.51 | −34.96 |
| TCL | 6.01 | −2.08 | 2.55 | −143.32 | −29.63 | −222.35 | −39.86 |
| **3g** | 5.77 | −2.72 | 0.00 | −138.06 | −18.76 | −232.66 | −31.88 |
| **3c** | 5.71 | −3.06 | 0.38 | −130.46 | −11.49 | −208.52 | −34.13 |
| **3h** | 5.22 | −3.28 | 0.00 | −137.17 | −8.18 | −227.21 | −34.31 |
| **3d** | 5.17 | −2.78 | 0.26 | −136.09 | −11.88 | −226.20 | −34.61 |
| **3b** | 5.11 | −2.81 | 0.03 | −139.85 | −17.39 | −242.18 | −32.08 |
| **3t** | 4.96 | −4.17 | 0.08 | −158.76 | −17.23 | −284.79 | −36.62 |
| **3r** | 4.81 | −4.90 | 0.00 | −154.85 | −37.77 | −252.10 | −34.62 |
| **3u** | 4.32 | −0.95 | 0.00 | −100.64 | −62.42 | −165.71 | −31.43 |
| **3n** | 4.41 | −4.09 | 0.43 | −142.88 | −19.48 | −234.70 | −36.55 |
| **3s** | 4.12 | −4.61 | 0.34 | −149.89 | −17.57 | −279.36 | −36.70 |
| **3m** | 4.01 | −3.95 | 0.03 | −155.67 | −14.77 | −256.26 | −34.37 |
| **3p** | 3.84 | −4.26 | 0.00 | −151.19 | −21.11 | −260.02 | −37.27 |
| **3o** | 3.83 | −4.48 | 0.25 | −146.64 | −14.69 | −242.54 | −36.18 |
| **3l** | 3.83 | −4.77 | 0.00 | −147.74 | −6.18 | −233.36 | −33.73 |
| **3q** | 3.62 | −4.90 | 0.76 | −164.44 | −25.16 | −254.40 | −37.40 |
| **3v** | 3.41 | −0.86 | 0.00 | −93.47 | −33.87 | −148.45 | −31.42 |
| **3i** | 3.02 | −0.85 | 0.00 | −89.69 | −49.44 | −143.10 | −31.89 |
| **3w** | 2.77 | −1.24 | 0.00 | −95.76 | −55.27 | −146.41 | −32.91 |

[a] C score (consensus score) scoring functions for ranking the affinity of ligands bound to the active site of a receptor

[b] Crash score revealing the inappropriate penetration into the binding site. Crash scores close to 0 are favorable. Negative numbers indicate penetration

[c] Polar indicating the contribution of the polar interactions to the total score

[d] D score for charge and van der Waals interactions between the protein and the ligand (Kuntz *et al.*, 1982)

[e] PMF score indicating Helmholtz free energies of interactions for protein–ligand atom pairs (Potential of Mean Force, PMF) (Muegge and Martin, 1999)

[f] G score for hydrogen bonding, complex (ligand–protein), and internal (ligand–ligand) energies (Jones *et al.*, 1997)

[g] Chem score points for H-bonding, lipophilic contact, and rotational entropy, along with an intercept term (Eldridge *et al.*, 1997)

Leco TruSpec CHNS Analyzer) for C, H and N fall within 0.4 % of the theoretical data. Thin-layer chromatography (TLC) was performed on pre-coated TLC sheets of silica gel 60 F254 (Merck, Darmstadt, Germany) visualized by long- and short-wavelength UV lamps. Chromatographic purifications were done on Merck aluminum oxide (70–230 mesh) and Merck silica gel (70–230 mesh).

### General procedure for synthesis of 2,5-dimethyl-substitutedphenyl-1*H*-pyrrole derivatives 2a–w

An equimolar quantity of different substituted aniline (0.1 mol), **1a–w** was dissolved in dry acetic acid containing 2,5-hexanedione (0.1 mol) and refluxed for 45 min at 100–115 °C. The mixture was cooled and poured slowly onto crushed ice cubes under stirring. The mixture was filtered, washed with water, dried and recrystallized using a suitable solvent.

### General procedure for synthesis of 2,5-dimethyl-substitutedphenyl-1*H*-pyrrole-3-carbaldehydes 3a–k and 3u

Vilsmeier–Haack reagent was prepared by adding phosphoryl chloride (10.5 equivalent) in dimethyl formamide (25 equivalent) at 0 °C with stirring. Then, 1 equivalent of

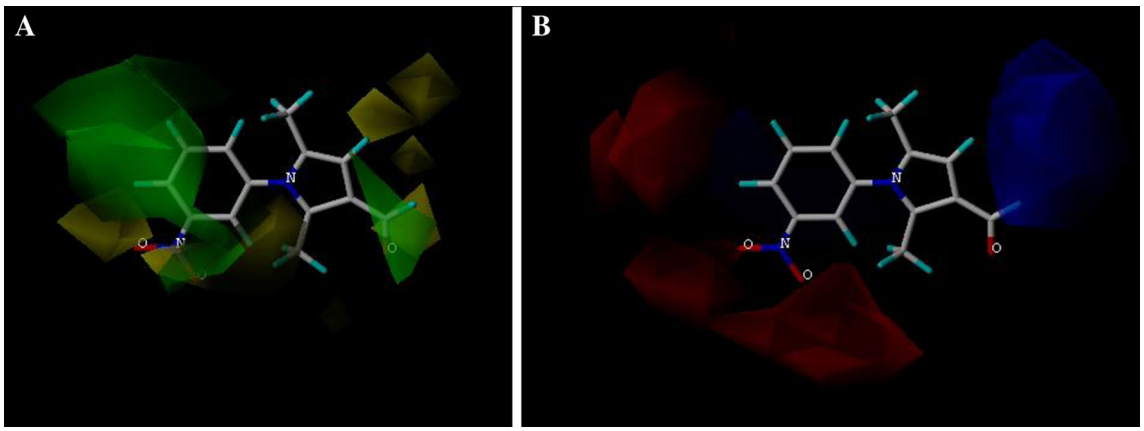


**Fig. 5** CoMFA contour map of final analysis with 2 Å grid spacing (compound **3f**). **a** Steric contour map. *Green contour* refers to sterically favored regions; *yellow contour* indicates sterically disfavored areas. **b** Electrostatic contour map. *Blue contours* refer to the region where positively charged substituents are favored; *red contours* indicate the regions where negatively charged substituents are favored (Color figure online)

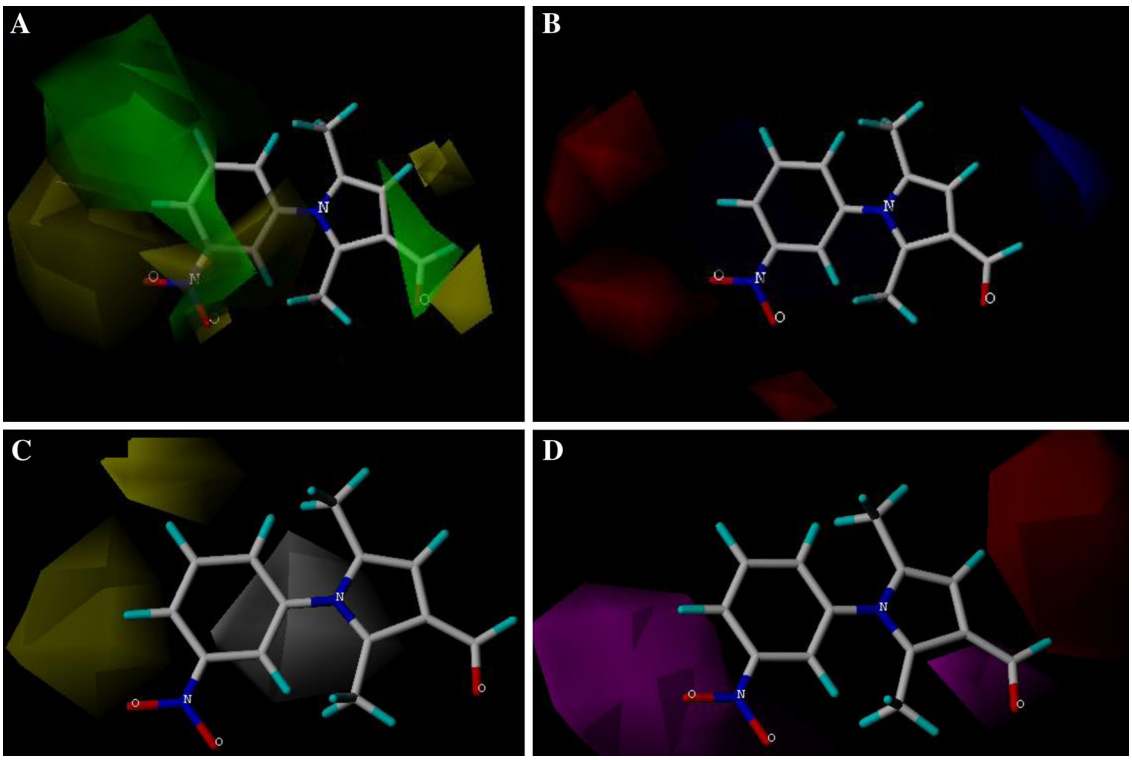


**Fig. 6** Contour maps of final CoMSIA analysis with 2 Å grid spacing (compound **2f**). **a** Steric contour maps, *green contours* (0.07 level) refer to sterically favored region; *yellow contours* (0.14 level) indicate disfavored areas. **b** *Blue contours* (2.43 level) refer to regions where negatively charged substituents are disfavored; *red contours* (10.95 level) indicate the regions where negatively charged substituent are favored. **c** Hydrophobic contour maps, *white contours* (1.05 level) refer to regions where hydrophilic substituents are favored; *yellow contours* (1.59 level) indicate the regions where hydrophobic substituent's favored. **d** H-bond acceptor contour map, magenta contours (0.59 level) encompass regions where hydrogen-bond donors on the receptor are expected. *Red contours* (2.51 level) refer to areas where hydrogen-bond on the receptor decrease the affinity (Color figure online)

**2a**–**k** and **2u** was added to the reagent and stirred at 0 °C for 30 min. The mixture was further stirred for 3–4 h at 100 °C (45–50 °C for 2 h in case of compound **3g**). After cooling, the mixture was diluted with cold water and basified with 1 M NaOH solution. The separated solid was collected, washed with water, dried and purified by column chromatography (pet. ether/chloroform/methanol 6:3:1).

**Table 4** Actual and predictive (Pred.) activities (pMIC) with residual ($\delta$) values for training and test set compounds using the 3D-QSAR model

| | Actual | CoMFA | | CoMSIA | |
|---|---|---|---|---|---|
| | | Pred. | $\Delta$ | Pred. | $\delta$ |
| *Training set compounds* | | | | | |
| **3a** | 5.5052 | 5.6024 | −0.0972 | 5.5963 | −0.0911 |
| **3b** | 5.5052 | 5.5002 | 0.0050 | 5.5027 | 0.0025 |
| **3c** | 5.2041 | 5.0300 | 0.1741 | 5.0276 | 0.1765 |
| **3f** | 5.2041 | 5.2061 | −0.0020 | 5.1058 | 0.0983 |
| **3h** | 4.9031 | 5.0558 | −0.1527 | 5.0483 | −0.1452 |
| **3j** | 5.2041 | 5.2130 | −0.0089 | 5.2089 | −0.0048 |
| **3k** | 5.5052 | 5.4772 | 0.0280 | 5.4863 | 0.0189 |
| **3m** | 5.2041 | 5.1884 | 0.0157 | 5.2057 | −0.0016 |
| **3n** | 4.9031 | 4.7519 | 0.1512 | 4.7567 | 0.1464 |
| **3o** | 4.9031 | 4.7800 | 0.1231 | 4.7794 | 0.1237 |
| **3q** | 5.2041 | 5.1073 | 0.0968 | 5.1173 | 0.0868 |
| **3t** | 4.9031 | 5.0862 | −0.1831 | 5.0993 | −0.1962 |
| **3u** | 4.6021 | 4.6936 | −0.0915 | 4.6751 | −0.073 |
| **3w** | 4.6021 | 4.5285 | 0.0736 | 4.5377 | 0.0644 |
| **3e** | 5.2041 | 5.0169 | 0.1872 | 5.0149 | 0.1892 |
| **3h** | 4.9031 | 5.1128 | −0.2097 | 5.0995 | −0.1964 |
| **3r** | 4.301 | 4.5622 | −0.2612 | 4.5495 | −0.2485 |
| **3v** | 4.9031 | 4.7795 | 0.1236 | 4.7785 | 0.1246 |
| **3i** | 4.6021 | 4.7716 | −0.1695 | 4.7737 | −0.1716 |
| *Test set compounds* | | | | | |
| **3d** | 5.2041 | 5.0615 | 0.1426 | 5.0193 | 0.1848 |
| **3s** | 5.2041 | 5.0496 | 0.1545 | 4.9694 | 0.2347 |
| **3l** | 5.2041 | 5.2885 | −0.0844 | 5.3325 | −0.1284 |
| **3p** | 4.9031 | 4.7406 | 0.1625 | 5.0324 | −0.1293 |
| **3g** | 4.6021 | 4.8295 | −0.2274 | 4.4898 | 0.1123 |

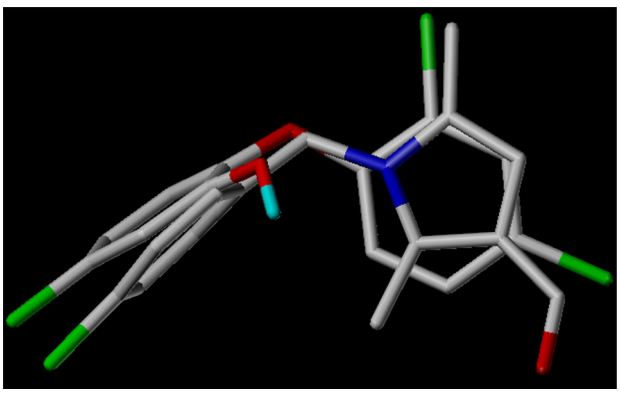

**Fig. 7** Comparison of size of pharmacophore which shows better fitting of compound **3k** than triclosan in receptor cavity

### 2,5-Dimethyl-1-(3-nitrophenyl)-1*H*-pyrrole-3-carbaldehyde (3a)

Compound **3a** was obtained as yellow solid. Yield 70 %; M.p. 140–142 °C; IR (KBr) $\nu_{max}$ 3084, 1530, 1482 (Ar–H), 1646 (C=O), 1485 (asym $NO_2$), 1315 (sym $NO_2$) $cm^{-1}$; $^1H$ NMR ($CDCl_3$, 400 MHz): $\delta = 2.00$ (s, 3H, pyrrole-$C_5$–$CH_3$), 2.29 (s, 3H, pyrrole-$C_2$–$CH_3$), 6.33 (d, 1H, pyrrole-$C_4$–H), 7.85–8.38 (m, 4H, phenyl-$C_2$, $C_4$, $C_5$, $C_6$–H), 9.83 (s, 1H, pyrrole-$C_3$–CHO); $^{13}C$ NMR ($CDCl_3$, 75 MHz): $\delta = 11.33$ (pyrrole-$C_5$–$CH_3$), 12.75 (pyrrole-$C_2$–$CH_3$), 106.91 (pyrrole-$C_3$ and $C_4$), 122.53 (phenyl-$C_2$), 123.29 (phenyl-$C_4$), 123.90 (phenyl-$C_6$), 130.64 (phenyl-$C_4$), 130.68 (pyrrole-$C_5$), 134.17 (pyrrole-$C_2$), 138.17 (phenyl-$C_3$), 148.87 (phenyl-$C_1$), 185.36 (pyrrole-$C_3$–CHO); MS (ESI): *m/z* found 245.10 [$M^+ + 1$]; calcd. 244.24; Anal. Calcd. for $C_{13}H_{12}N_2O_3$: C, 63.93; H, 4.95; N, 11.47. Found: C, 63.91; H, 4.94; N, 11.45.

### 2,5-Dimethyl-1-(4-nitrophenyl)-1*H*-pyrrole-3-carbaldehyde (3b)

Compound **3b** was obtained as yellow solid. Yield 65 %; M.p. 133–135 °C; IR (KBr) $\nu_{max}$ 3077, 1595, 1496 (Ar–H), 1656 (C=O), 1492 (asym $NO_2$), 1325 (sym $NO_2$) $cm^{-1}$; $^1H$ NMR ($CDCl_3$, 400 MHz): $\delta = 2.03$ (s, 3H, pyrrole-$C_5$–

$CH_3$), 2.32 (s, 3H, pyrrole-$C_2$–$CH_3$), 6.43 (s, 1H, pyrrole-$C_4$–H), 7.41–7.45, 8.40–8.43 (m, 4H, phenyl-$C_2$, $C_3$, $C_5$, $C_6$–H), 9.90 (s, 1H, pyrrole-$C_3$–CHO); MS (ESI): *m/z* found 245.01 [$M^+ + 1$]; calcd. 244.24; Anal. Calcd. for $C_{13}H_{12}N_2O_3$: C, 63.93; H, 4.95; N, 11.47. Found: C, 63.91; H, 4.93; N, 11.45.

### 1-(4-Chlorophenyl)-2,5-dimethyl-1*H*-pyrrole-3-carbaldehyde (3c)

Compound **3c** was obtained as dark yellow solid. Yield 72 %; M.p. 190–200 °C; IR (KBr) $\nu_{max}$ 3077, 1596, 1496 (Ar–H), 1655 (C=O), 790 (Ar–Cl) $cm^{-1}$; $^1H$ NMR ($CDCl_3$, 400 MHz): $\delta = 1.98$ (d, 3H, pyrrole-$C_5$–$CH_3$), 2.27 (s, 3H, pyrrole-$C_2$–$CH_3$), 6.38 (d, 1H, pyrrole-$C_4$–H), 7.13–7.52 (m, 4H, phenyl-$C_2$, $C_3$, $C_5$, $C_6$–H), 9.87 (s, 1H, pyrrole-$C_3$–CHO); MS (ESI): *m/z* found 234.06 [$M^+ + 1$]; calcd. 233.69; Anal. Calcd. for $C_{13}H_{12}ClNO$: C, 66.81; H, 5.18; N, 5.99. Found: C, 66.79; H, 5.10; N, 5.95.

### 1-(3-Chlorophenyl)-2,5-dimethyl-1*H*-pyrrole-3-carbaldehyde (3d)

Compound **3d** was obtained as yellow solid. Yield 70 %; M.p. 150–154 °C; IR (KBr) $\nu_{max}$ 3068, 1606, 1477 (Ar–H), 1668 (C=O), 786 (Ar–Cl) $cm^{-1}$; $^1H$ NMR ($CDCl_3$, 400 MHz): $\delta = 1.93$ (s, 3H, pyrrole-$C_5$–$CH_3$), 2.23 (s, 3H, pyrrole-$C_2$–$CH_3$), 6.41 (s, 1H, pyrrole-$C_4$–H), 7.26–7.78 (m, 4H, phenyl-$C_2$, $C_4$, $C_5$, $C_6$–H), 9.89 (s, 1H, pyrrole $C_3$–CHO); MS (ESI): *m/z* 234.10 [$M^+ + 1$], 236.02 [$M^+ + 2$]; calcd. 233.69; Anal. Calcd. for $C_{13}H_{12}ClNO$: C, 66.81; H, 5.18; N, 5.99. Found: C, 66.78; H, 5.14; N, 5.97.

### 1-(4-Bromophenyl)-2,5-dimethyl-1*H*-pyrrole-3-carbaldehyde (3e)

Compound **3e** was obtained as yellow solid. Yield 71 %; M.p. 183–186 °C; IR (KBr) $\nu_{max}$ 3061, 1651, 1491 (Ar–H), 1668 (C=O), 684 (Ar–Br) $cm^{-1}$; $^1H$ NMR ($CDCl_3$, 400 MHz): $\delta = 1.56$ (s, 3H, pyrrole-$C_5$–$CH_3$), 2.30 (s, 3H, pyrrole-$C_2$–$CH_3$), 6.30 (s, H, pyrrole-$C_4$–H), 7.08–7.72 (m, 4H, phenyl-$C_2$, $C_3$, $C_5$, $C_6$–H), 10.36 (s, 1H, pyrrole-$C_3$–CHO); $^{13}C$ NMR ($CDCl_3$, 75 MHz): $\delta = 11.66$ (pyrrole-$C_2$ and $C_5$–$2CH_3$), 106.50 (pyrrole-$C_3$ and $C_4$), 120.51 (phenyl-$C_4$), 124.11 (phenyl-$C_2$ and $C_6$), 129.63 (pyrrole-$C_5$), 132.90 (phenyl-$C_5$), 133.38 (phenyl-$C_3$), 134.46 (pyrrole-$C_2$), 139.45 (phenyl-$C_1$), 187.22 (pyrrole-$C_3$–CHO); MS (ESI): *m/z* found 279.10 [$M^+ + 1$], 281 [$M^+ + 2$]; calcd. 278.14; Anal. Calcd. for $C_{13}H_{12}BrNO$: C, 56.14; H, 4.35; N, 5.04. Found: C, 56.16; H, 4.32; N, 5.02.

### 2,5-Dimethyl-1-(2-nitrophenyl)-1*H*-pyrrole-3-carbaldehyde (3f)

Compound **3f** was obtained as yellow solid. Yield 55 %; M.p. 88–90 °C; IR (KBr) $\nu_{max}$ 3046, 1604, 1491 (Ar–H), 1655 (C=O), 1490 (asym $NO_2$), 1331 (sym $NO_2$) $cm^{-1}$; $^1H$ NMR ($CDCl_3$, 400 MHz): $\delta = 1.93$ (s, 3H, pyrrole-$C_5$–$CH_3$), 2.24 (s, 3H, pyrrole-$C_2$–$CH_3$), 6.41 (d, 1H, pyrrole-$C_4$–H), 7.38–8.10 (m, 4H, phenyl-$C_3$, $C_4$, $C_5$, $C_6$–H), 9.87 (s, 1H, pyrrole-$C_3$–CHO); $^{13}C$ NMR ($CDCl_3$, 75 MHz): $\delta = 10.93$ (pyrrole-$C_5$–$CH_3$), 12.21 (pyrrole-$C_2$–$CH_3$), 106.78 (pyrrole-$C_3$ and $C_4$), 122.67 (phenyl-$C_6$), 125.38 (phenyl-$C_3$ and $C_4$), 130.53 (pyrrole-$C_5$), 131.28 (phenyl-$C_1$), 133.96 (pyrrole-$C_2$ and phenyl-$C_5$), 138.84 (phenyl-$C_2$), 185.35 (pyrrole-$C_3$–CHO); MS (ESI): *m/z* found 245.10 [$M^+ + 1$]; calcd. 244.24; Anal. Calcd. for $C_{13}H_{12}N_2O_3$: C, 63.93; H, 4.95; N, 11.47. Found: C, 63.92; H, 4.90; N, 11.41.

### 1-(4-Methoxyphenyl)-2,5-dimethyl-1*H*-pyrrole-3-carbaldehyde (3g)

Compound **3g** was obtained as yellow solid. Yield 82 %; M.p. 136–138 °C; IR (KBr) $\nu_{max}$ 3056, 1608, 1466 (Ar–H), 1651 (C=O), 1255 (C–O) $cm^{-1}$; $^1H$ NMR ($CDCl_3$, 400 MHz): $\delta = 1.97$ (s, 3H, pyrrole-$C_5$–$CH_3$), 2.27 (s, 3H, pyrrole-$C_2$–$CH_3$), 3.88 (s, 3H, $OCH_3$), 6.37 (d, 1H, pyrrole-$C_4$–H), 7.00–7.26 (m, 4H, phenyl-$C_2$, $C_3$, $C_5$, $C_6$–H), 9.85 (s, 1H, pyrrole-$C_3$–CHO); $^{13}C$ NMR ($CDCl_3$, 75 MHz): $\delta = 11.20$ (pyrrole-$C_5$–$CH_3$), 12.64 (pyrrole-$C_2$–$CH_3$), 55.56 ($OCH_3$), 105.51 (pyrrole-$C_4$), 114.70 (pyrrole-$C_3$), 121.74 (phenyl-$C_3$ and $C_5$), 128.97 (pyrrole-$C_5$), 129.58 (phenyl-$C_2$ and $C_6$), 131.33 (phenyl-$C_1$), 139.30 (pyrrole-$C_2$), 159.72 (phenyl-$C_4$), 185.26 (pyrrole-$C_3$–CHO); MS (ESI): *m/z* found 230.11 [$M^+ + 1$]; calcd. 229.27; Anal. Calcd. for $C_{14}H_{15}NO_2$: C, 73.34; H, 6.59; N, 6.11. Found: C, 73.32; H, 6.55; N, 6.15.

### 1-(3-Bromophenyl)-2,5-dimethyl-1*H*-pyrrole-3-carbaldehyde (3h)

Compound **3h** was obtained as yellow solid. Yield 68 %; M.p. 80–82 °C; IR (KBr) $\nu_{max}$ 3061, 1651, 1491 (Ar–H), 1668 (C=O), 698 (Ar–Br) $cm^{-1}$; $^1H$ NMR ($CDCl_3$, 400 MHz): $\delta = 1.93$ (s, 3H, pyrrole-$C_5$–$CH_3$), 2.23 (s, 3H, pyrrole-$C_2$–$CH_3$), 6.41 (s, 1H, pyrrole-$C_4$–H), 7.26–7.78 (m, 4H, phenyl-$C_2$, $C_4$, $C_5$, $C_6$–H), 9.89 (s, 1H, pyrrole-$C_3$–CHO); MS (ESI): *m/z* found 278.01 [$M^+$], 280.04 [$M^+ + 2$]; calcd. 278.14; Anal. Calcd. for $C_{13}H_{12}BrNO$: C, 56.14; H, 4.35; N, 5.04. Found: C, 56.13; H, 4.31; N, 5.00.

### 1-(2-Bromophenyl)-2,5-dimethyl-1*H*-pyrrole-3-carbaldehyde (3i)

Compound **3i** was obtained as yellow solid. Yield 50 %; M.p. 68–70 °C; IR (KBr) $\nu_{max}$ 3034, 1584, 1479 (Ar–H), 1653 (C=O), 695 (Ar–Br) $cm^{-1}$; $^1H$ NMR ($CDCl_3$, 400 MHz): $\delta = 1.93$ (s, 3H, pyrrole-$C_5$–$CH_3$), 2.23 (s, 3H, pyrrole-$C_2$–$CH_3$), 6.41 (d, H, pyrrole-$C_4$–H), 7.26–7.78 (m, 4H, phenyl-$C_3$, $C_4$, $C_5$, $C_6$–H), 9.89 (s, 1H, pyrrole-$C_3$–CHO); $^{13}C$ NMR ($CDCl_3$, 75 MHz): $\delta = 10.93$ (pyrrole-$C_5$–$CH_3$), 12.30 (pyrrole-$C_2$–$CH_3$), 105.86 (pyrrole-$C_3$), 113.40 (pyrrole-$C_4$ and phenyl-$C_2$), 122.12 (phenyl-$C_6$), 128.66 (phenyl-$C_4$ and pyrrole-$C_5$), 130.09 (phenyl-$C_5$), 130.84 (phenyl-$C_3$), 133.78 (pyrrole-$C_2$), 139.10 (phenyl-$C_1$), 185.32 (pyrrole-$C_3$–CHO); MS (ESI): *m/z* found 278.01 [$M^+$], 280.21 [$M^+ + 2$]; calcd. 278.14; Anal. Calcd. for $C_{13}H_{12}BrNO$: C, 56.14; H, 4.35; N, 5.04. Found: C, 56.15; H, 4.34; N, 5.00.

### 1-(4-Chlorobenzyl)-2,5-dimethyl-1*H*-pyrrole-3-carbaldehyde (3j)

Compound **3j** was obtained as yellow solid. Yield 71 %; M.p. 78–80 °C; IR (KBr) $\nu_{max}$ 3099, 1536, 1477 (Ar–H), 1643 (C=O), 797 (Ar–Cl) $cm^{-1}$; $^1H$ NMR ($CDCl_3$, 400 MHz): $\delta = 2.12$ (s, 3H, pyrrole-$C_5$–$CH_3$), 2.41 (s, 3H, pyrrole-$C_2$–$CH_3$), 5.01 (s, 2H, benzyl-$CH_2$), 6.36 (s, 1H, pyrrole-$C_4$–H), 6.82–7.31 (m, 4H, phenyl-$C_2$, $C_3$, $C_5$, $C_6$–H), 9.84 (s, 1H, pyrrole-$C_3$–CHO); $^{13}C$ NMR ($CDCl_3$, 75 MHz): $\delta = 11.23$ (pyrrole-$C_5$–$CH_3$), 12.67 (pyrrole-$C_2$–$CH_3$), 106.16 (pyrrole-$C_3$ and $C_4$), 122.11 (phenyl-$C_2$ and $C_6$), 129.31 (pyrrole-$C_5$), 129.90 (phenyl-$C_3$ and $C_5$), 130.86 (phenyl-$C_4$), 135.02 (pyrrole-$C_2$), 138.61 (phenyl-$C_1$), 185.29 (pyrrole-$C_3$–CHO); MS (ESI): *m/z* found 248.08 [$M^+ + 1$], 250 [$M^+ + 2$]; calcd. 247.72; Anal. Calcd. for $C_{14}H_{14}ClNO$: C, 67.88; H, 5.70; N, 5.65. Found: C, 67.82; H, 5.72; N, 5.63.

### 1-(3-Chlorobenzyl)-2,5-dimethyl-1*H*-pyrrole-3-carbaldehyde (3k)

Compound **3k** was obtained as yellow solid. Yield 65 %; M.p. 88–90 °C; IR (KBr) $\nu_{max}$ 2920, 1594, 1475 (Ar–H), 1647 (C=O), 788 (Ar–Cl) $cm^{-1}$; $^1H$ NMR ($CDCl_3$, 400 MHz): $\delta = 2.13$ (s, 3H, pyrrole-$C_5$–$CH_3$), 2.42 (s, 3H, pyrrole-$C_2$–$CH_3$), 5.02 (s, 2H, benzyl-$CH_2$), 6.37 (d, 1H, pyrrole-$C_4$–H), 6.73–7.26 (m, 4H, phenyl-$C_2$, $C_4$, $C_5$, $C_6$–H), 9.85 (s, 1H, pyrrole-$C_3$–CHO); $^{13}C$ NMR ($CDCl_3$, 75 MHz): $\delta = 10.52$ (pyrrole-$C_5$–$CH_3$), 12.18 (pyrrole-$C_2$–$CH_3$), 106.66 (pyrrole-$C_3$ and $C_4$), 121.93 (phenyl-$C_2$ and $C_6$), 125.73 (phenyl-$C_4$), 127.97 (pyrrole-$C_5$), 130.39 (phenyl-$C_5$), 135.12 (phenyl-$C_3$ and pyrrole-$C_2$), 138.58 (phenyl-$C_1$), 185.19 (pyrrole-$C_3$–CHO); MS (ESI): *m/z* found 248.08 [$M^+ + 1$], 250.04 [$M^+ + 2$]; calcd. 247.72; Anal. Calcd. for $C_{14}H_{14}ClNO$: C, 67.88; H, 5.70; N, 5.65. Found: C, 67.84; H, 5. 68; N, 5.61.

### 1-(3-Methoxyphenyl)-2,5-dimethyl-1*H*-pyrrole-3-carbaldehyde (3u)

Compound **3u** was obtained as yellow solid. Yield 89 %; M.p. 119–122 °C; IR (KBr) $\nu_{max}$ 3056, 1600, 1470 (Ar–H), 1668 (C=O), 1261 (C–O) $cm^{-1}$; $^1H$ NMR ($CDCl_3$, 400 MHz): $\delta = 1.92$ (s, 3H, pyrrole-$C_5$–$CH_3$), 2.27 (s, 3H, pyrrole-$C_2$–$CH_3$), 3.51 (s, 3H, $OCH_3$), 7.65–8.30 (m, 4H, phenyl-$C_3$, $C_4$, $C_5$, $C_6$–H), 10.35 (s, 1H, pyrrole-$C_3$–CHO); MS (ESI): *m/z* found 230.11 [$M^+ + 1$]; calcd. 229.27; Anal. Calcd. for $C_{14}H_{15}NO_2$: C, 73.34; H, 6.59; N, 6.11. Found: C, 73.31; H, 6.57; N, 6.10.

### General procedure for the synthesis of 2,5-dimethylsubstitutedphenyl-1*H*-pyrrole-3,4-dicarbaldehydes 3l–t and 3v–w

Phosphoryl chloride (25 equivalent) was added drop wise to DMF (23 equivalent) at 0 °C and the reaction was stirred for 1 h to which 1 equivalent of **2l–t**, **2v–w** was added. The final mixture was stirred to 100 °C for 3–4 h (45–50 °C up to 2 h in case of **3r**). Solution thus obtained was cooled and poured in cold water. Basic workout was performed with 1 M NaOH. The separated solid was collected, washed with water, dried and purified by column chromatography (pet. ether/chloroform/methanol 6:3:1).

### 2,5-Dimethyl-1-(3-nitrophenyl)-1*H*-pyrrole-3,4-dicarbaldehyde (3l)

Compound **3l** was obtained as brown solid. Yield 71 %; M.p. 148–150 °C; IR (KBr) $\nu_{max}$ 3077, 1595, 1496 (Ar–H), 1655 (C=O), 1496 (asym $NO_2$), 1340 (sym $NO_2$) $cm^{-1}$; $^1H$ NMR ($CDCl_3$, 400 MHz): $\delta = 2.32$ (s, 6*H*, pyrrole-$C_5$, $C_2$–$CH_3$), 7.79–8.47 (m, 4H, phenyl-$C_2$, $C_4$, $C_5$, $C_6$–H), 10.32 (s, 2H, pyrrole-$C_3$, $C_4$–CHO); MS (ESI): *m/z* found 273.08 [$M^+ + 1$]; calcd. 272.25; Anal. Calcd. for $C_{14}H_{12}N_2O_4$: C, 61.76; H, 4.44; N, 10.29. Found: C, 61.74; H, 4.41; N, 10.27.

### 2,5-Dimethyl-1-(4-nitrophenyl)-1*H*-pyrrole-3,4-dicarbaldehyde (3m)

Compound **3m** was obtained as brown solid. Yield 76 %; M.p. 110 °C; IR (KBr) $\nu_{max}$ 3071.56, 1602.16, 1484.36 (Ar–H), 1672.33 (C=O), 1496.65 (asym $NO_2$), 1340.54 (sym $NO_2$) $cm^{-1}$; $^1H$ NMR ($CDCl_3$, 400 MHz): $\delta = 2.31$ (s, 6*H*, pyrrole $C_5$, $C_2$–$CH_3$), 7.70–8.47 (m, 4H, phenyl-$C_2$, $C_3$, $C_5$, $C_6$–H), 10.31 (s, 2H, pyrrole-$C_3$, $C_4$–CHO); $^{13}C$

NMR ($CDCl_3$, 75 MHz): $\delta = 11.73$ (pyrrole-$C_2$ and $C_5$–$2CH_3$), 107.66 (pyrrole-$C_3$ and $C_4$), 120.84 (phenyl-$C_2$ and $C_6$), 124.83 (phenyl-$C_3$ and $C_5$), 134.05 (pyrrole-$C_2$ and $C_5$), 139.08 (phenyl-$C_1$ and $C_4$), 187.11 (pyrrole-$C_3$ and $C_4$–2CHO); MS (ESI): *m/z* found 273.14 [$M^+ + 1$]; calcd. 272.25; Anal. Calcd. for $C_{14}H_{12}N_2O_4$: C, 61.76; H, 4.44; N, 10.29. Found: C, 61.74; H, 4.44; N, 10.27.

### 1-(4-Chlorophenyl)-2,5-dimethyl-1*H*-pyrrole-3,4-dicarbaldehyde (3n)

Compound **3n** was obtained as brown solid. Yield 80 %; M.p. 112–115 °C; IR (KBr) $\nu_{max}$ 2921, 1594, 1495 (Ar–H), 1650 (C=O), 783 (Ar–Cl) $cm^{-1}$; $^1H$ NMR ($CDCl_3$, 400 MHz): $\delta = 2.30$ (s, 6*H*, pyrrole-$C_5$, $C_2$–$CH_3$), 7.14–7.57 (m, 4H, phenyl-$C_2$, $C_3$, $C_5$, $C_6$–H), 10.36 (s, 2H, pyrrole-$C_3$, $C_4$–CHO); MS (ESI): *m/z* found 262.06 [$M^+ + 1$], 264.01 [$M^+ + 2$]; calcd. 261.70; Anal. Calcd. for $C_{14}H_{12}ClNO_2$: C, 64.25; H, 4.62; N, 5.35. Found: C, 64.24; H, 4.61; N, 5.31.

### 1-(3-Chlorophenyl)-2,5-dimethyl-1*H*-pyrrole-3,4-dicarbaldehyde (3o)

Compound **3o** was obtained as brown solid. Yield 72 %; M.p. 177–180 °C; IR (KBr) $\nu_{max}$ 3074, 1592, 1484 (Ar–H), 1670 (C=O), 798 (Ar–Cl) $cm^{-1}$; $^1H$ NMR ($CDCl_3$, 400 MHz): $\delta = 2.31$ (s, 6*H*, pyrrole-$C_5$, $C_2$–$CH_3$), 7.11–7.57 (m, 4H, phenyl-$C_2$, $C_4$, $C_5$, $C_6$–H), 10.36 (s, 2H, pyrrole-$C_3$, $C_4$–CHO); $^{13}C$ NMR ($CDCl_3$, 75 MHz): $\delta = 11.67$ (pyrrole-$C_2$ and $C_5$–$2CH_3$), 113.66 (pyrrole-$C_3$ and $C_4$), 120.50 (phenyl-$C_2$), 126.23 (phenyl-$C_6$), 128.23 (phenyl-$C_4$), 130.26 (phenyl-$C_5$), 131.07 (phenyl-$C_3$), 135.80 (pyrrole-$C_2$ and $C_5$), 139.45 (phenyl-$C_1$), 187.24 (pyrrole-$C_3$ and $C_4$–2CHO); MS (ESI): *m/z* found 262.06 [$M^+ + 1$], 264.24 [$M^+ + 2$]; calcd. 261.70; Anal. Calcd. for $C_{14}H_{12}ClNO_2$: C, 64.25; H, 4.62; N, 5.35. Found: C, 64.24; H, 4.61; N, 5.31.

### 1-(4-Bromophenyl)-2,5-dimethyl-1*H*-pyrrole-3,4-dicarbaldehyde (3p)

Compound **3p** was obtained as brown solid. Yield 78 %; M.p. 109–110 °C; IR (KBr) $\nu_{max}$ 3047, 1587, 1490 (Ar–H), 1653 (C=O), 695 (Ar–Br) $cm^{-1}$; $^1H$ NMR ($CDCl_3$, 400 MHz): $\delta = 1.98$ (s, 3H, pyrrole-$C_5$–$CH_3$), 2.28 (s, 3H, pyrrole-$C_2$–$CH_3$), 7.08–7.67 (m, 4H, phenyl-$C_2$, $C_3$, $C_5$, $C_6$–H), 9.86 (s, 2H, pyrrole-$C_3$, $C_4$-CHO); $^{13}C$ NMR ($CDCl_3$, 75 MHz): $\delta = 11.24$ (pyrrole-$C_2$ and $C_5$–$2CH_3$), 106.20 (pyrrole-$C_3$ and $C_4$), 122.14 (phenyl-$C_4$), 123.03 (phenyl-$C_2$ and $C_6$), 132.90 (phenyl-$C_3$ and $C_5$), 136.00 (pyrrole-$C_2$ and $C_5$), 138.55 (phenyl-$C_1$), 185.30 (pyrrole-$C_3$ and $C_4$–2CHO); MS (ESI): *m/z* found 306.12 [$M^+$], 308.21 [$M^+ + 2$]; calcd. 306.15; Anal. Calcd. for $C_{14}H_{12}BrNO_2$: C, 54.92; H, 3.95; N, 4.58. Found: C, 54.92; H, 3.94; N, 4.55.

### 2,5-Dimethyl-1-(2-nitrophenyl)-1*H*-pyrrole-3,4-dicarbaldehyde (3q)

Compound **3q** was obtained as brown solid. Yield 48 %; M.p. 85–90 °C; IR (KBr) $\nu_{max}$ 3057, 1601, 1475 (Ar–H), 1668 (C=O), 1490 (asym $NO_2$), 1324 (sym $NO_2$) $cm^{-1}$; $^1H$ NMR ($CDCl_3$, 400 MHz): $\delta = 2.56$ (s, 6*H*, pyrrole-$C_5$, $C_2$–$CH_3$), 7.88–8.32 (m, 4H, phenyl-$C_3$, $C_4$, $C_5$, $C_6$–H), 10.39 (s, 2H, pyrrole-$C_3$, $C_4$–CHO); MS (ESI): *m/z* found 273.14 [$M^+ + 1$]; calcd. 272.25; Anal. Calcd. for $C_{14}H_{12}N_2O_4$: C, 61.76; H, 4.44; N, 10.29. Found: C, 61.74; H, 4.39; N, 10.27.

### 1-(4-Methoxyphenyl)-2,5-dimethyl-1*H*-pyrrole-3,4-dicarbaldehyde (3r)

Compound **3r** was obtained as brown solid. Yield 88 %; M.p. 90–93 °C; IR (KBr) $\nu_{max}$ 3057, 1601, 1475 (Ar–H), 1668 (C=O), 1265 (C–O) $cm^{-1}$; $^1H$ NMR ($CDCl_3$, 400 MHz): $\delta = 1.97$ (s, 3H, pyrrole-$C_5$–$CH_3$), 2.27 (s, 3H, pyrrole-$C_2$–$CH_3$), 3.88 (s, 3H, $OCH_3$), 7.00–7.26 (m, 4H, phenyl-$C_3$, $C_4$, $C_5$, $C_6$–H), 9.84 (s, 2H, pyrrole-$C_3$, $C_4$–CHO); $^{13}C$ NMR ($CDCl_3$, 75 MHz): $\delta = 11.21$ (pyrrole-$C_2$ and $C_5$–$2CH_3$), 55.56 ($OCH_3$), 114.70 (pyrrole-$C_3$ and $C_4$), 121.75 (phenyl-$C_3$ and $C_5$), 128.98 (phenyl-$C_2$ and $C_6$), 129.59 (phenyl-$C_1$), 131.31 (pyrrole-$C_2$ and $C_5$), 159.72 (phenyl-$C_4$), 185.26 (pyrrole-$C_3$ and $C_4$–2CHO); MS (ESI): *m/z* found 257.01 [$M^+$]; calcd. 257.28; Anal. Calcd. for $C_{15}H_{15}NO_3$: C, 70.02; H, 5.40; N, 5.44. Found: C, 70.00; H, 5.41; N, 5.42.

### 1-(4-Chlorobenzyl)-2,5-dimethyl-1*H*-pyrrole-3,4-dicarbaldehyde (3s)

Compound **3s** was obtained as brown solid. Yield 72 %; M.p. 78–80 °C; IR (KBr) $\nu_{max}$ 3099, 1536, 1477 (Ar–H), 1643 (C=O), 781 (Ar–Cl) $cm^{-1}$; $^1H$ NMR ($CDCl_3$, 400 MHz): $\delta = 2.12$ (s, 6*H*, pyrrole-$C_5$, $C_2$–$CH_3$), 5.08 (s, 2H, benzyl-$CH_2$), 7.29–7.34 (m, 4H, phenyl-$C_2$, $C_3$, $C_5$, $C_6$–H), 9.84 (s, 1H, pyrrole-$C_3$–CHO), 10.35 (s, 1H, pyrrole-$C_4$–CHO); MS (ESI): *m/z* found 276.07 [$M^+ + 1$], 278.01 [$M^+ + 2$]; calcd. 275.73; Anal. Calcd. for $C_{15}H_{14}ClNO_2$: C, 65.34; H, 5.12; N, 5.08. Found: C, 65.31; H, 5.14; N, 5.05.

### 1-(2-Chlorobenzyl)-2,5-dimethyl-1*H*-pyrrole-3,4-dicarbaldehyde (3t)

Compound **3t** was obtained as brown solid. Yield 68 %; M.p. 128–130 °C; IR (KBr) $\nu_{max}$ 2917, 1584, 1479 (Ar–H),

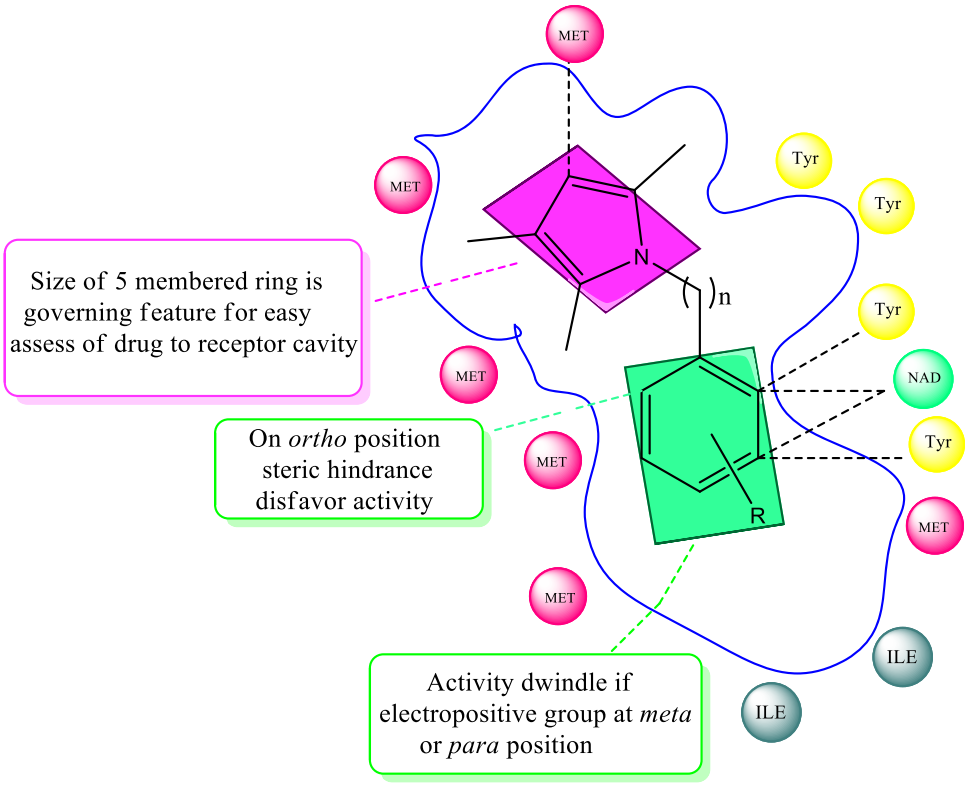


**Fig. 8** Pictorial presentation of structural activity relationship

1653 (C=O), 785 (Ar–Cl) $cm^{-1}$; $^1H$ NMR ($CDCl_3$, 400 MHz): $\delta = 2.45$ (s, 6*H*, pyrrole-$C_5$, $C_2$–$CH_3$), 5.15 (s, 2H, benzyl-$CH_2$), 7.19–7.46 (m, 4H, phenyl-$C_3$, $C_4$, $C_5$, $C_6$–H), 10.36 (s, 2H, pyrrole-$C_3$, $C_4$–CHO); $^{13}C$ NMR ($CDCl_3$, 75 MHz): $\delta = 10.63$ (pyrrole-$C_2$ and $C_5$–$2CH_3$), 44.59 ($CH_2$), 108.00 (pyrrole-$C_3$ and $C_4$), 125.81 (phenyl-$C_5$), 127.79 (phenyl-$C_4$), 129.38 (phenyl-$C_3$), 129.88 (phenyl-$C_6$), 131.97 (pyrrole-$C_2$ and $C_5$), 132.55 (phenyl-$C_2$), 138.98 (phenyl-$C_1$), 187.14 (pyrrole-$C_3$ and $C_4$–2CHO); MS (ESI): *m/z* found 276.07 [$M^+ + 1$], 278.25 [$M^+ + 2$]; calcd. 275.73; Anal. Calcd. for $C_{15}H_{14}ClNO_2$: C, 65.34; H, 5.12; N, 5.08. Found: C, 65.31; H, 5.14; N, 5.06.

### 1-(3-Bromophenyl)-2,5-dimethyl-1*H*-pyrrole-3,4-dicarbaldehyde (3v)

Compound **3v** was obtained as brown solid. Yield 65 %; M.p. 67–70 °C; IR (KBr) $\nu_{max}$ 2917, 1585, 1478 (Ar–H), 1653 (C=O), 690 (Ar–Br) $cm^{-1}$; $^1H$ NMR ($CDCl_3$, 400 MHz): $\delta = 2.31$ (d, 6*H*, pyrrole-$C_5$, $C_2$–$CH_3$), 7.15–7.72 (m, 4H, phenyl-$C_2$, $C_4$, $C_5$, $C_6$–H), 10.36 (s, 2H, pyrrole-$C_3$, $C_4$–CHO); $^{13}C$ NMR ($CDCl_3$, 75 MHz): $\delta = 11.68$ (pyrrole-$C_2$ and $C_5$–$2CH_3$), 113.10 (pyrrole-$C_3$ and $C_4$), 120.47 (phenyl-$C_2$), 123.48 (phenyl-$C_6$), 126.69 (phenyl-$C_3$), 130.85 (phenyl-$C_4$), 133.18 (phenyl-$C_5$), 136.72 (pyrrole-$C_2$ and $C_5$), 139.49 (phenyl-$C_1$), 187.23 (pyrrole-$C_3$ and $C_4$–2CHO); MS (ESI): *m/z* found 306.01 [$M^+$], 308.21 [$M^+ + 2$]; calcd. 306.15; Anal. Calcd. for $C_{14}H_{12}BrNO_2$: C, 54.92; H, 3.95; N, 4.58. Found: C, 54.92; H, 3.92; N, 4.54.

### 1-(2-Bromophenyl)-2,5-dimethyl-1*H*-pyrrole-3,4-dicarbaldehyde (3w)

Compound **3w** was obtained as brown solid. Yield 60 %; M.p. 65–68 °C; IR (KBr) $\nu_{max}$ 3001, 1600, 1474 (Ar–H), 1654 (C=O), 684 (Ar–Br) $cm^{-1}$; $^1H$ NMR ($CDCl_3$, 400 MHz): $\delta = 2.31$ (s, 6*H*, pyrrole-$C_5$, $C_2$–$CH_3$), 7.11–7.58 (m, 4H, phenyl-$C_3$, $C_4$, $C_5$, $C_6$–H), 10.36 (s, 2H, pyrrole-$C_3$, $C_4$–CHO); MS (ESI): *m/z* found 306.01 [$M^+$], 308.52 [$M^+ + 2$]; calcd. 306.15; Anal. Calcd. for $C_{14}H_{12}BrNO_2$: C, 54.92; H, 3.95; N, 4.58. Found: C, 54.91; H, 3.97; N, 4.57.

## Biological activities

### Antitubercular activity

The MIC values were determined for 2,5-dimethyl-1-(*o/m/p*-substitutedphenyl)-1*H*-pyrrole-3/4-carbaldehydes (**3a–i**, **3l–r** and **3u–w**), 2,5-dimethyl-1-(*o/m/p*-substitutedbenzyl)-1*H*-pyrrole-3/4-carbaldehydes (**3j–k**, **3s** and **3t**) against *M.*

*tuberculosis* strain $H_{37}Rv$ using the microplate Alamar Blue assay (MABA) (Franzblau *et al.* 1998). For MIC measurement, 200 µl of sterile deionzed water was added to all outer perimeter wells of sterile 96-well plate to minimize the evaporation losses of the medium during incubation. The 96-wells plate received 100 µl of the Middlebrook 7H9 broth, and serial dilution of compounds were made directly on the plate. The final drug concentrations tested were 100–0.2 µg/ml. Plates were covered and sealed with parafilm and incubated at 37 °C up to 5 days. Then, 25 µl of freshly prepared 1:1 mixture of Almar Blue reagent and 10 % Tween 80 was added to the plate and incubated for 24 h. A blue color in the well was interpreted as no bacterial growth and pink color was scored as growth. Table 1 reveals antitubercular activity in terms of MIC data.

## Summary of structure–activity relationship

During the development of drug design concept, our main aim was to design such type of hit molecule, which may easily penetrate to the enoyl-ACP reductase enzyme. Docking and 3D-QSAR models brought us closer to our hypothesis to conclude that five-membered rings are better choices than six-membered rings to improve antitubercular activity. To some extent, steric bulk at the 3rd position of pyrrole has increased the activity of compounds **3a**, **3b** and **3k**. To increase the interaction between drug and receptor, the orientation of aldehyde at the 3rd position of pyrrole was very significant (compound **3b**). The 3D-QSAR study helped us to conclude that increase in steric bulk at the 4th position of pyrrole is responsible to cause a dip in MIC values (compound **3l**–**q**) and also the electropositive group at the benzene ring connected with dialdehydic pyrrole has decreased the antitubercular activity up to its lowest limit (Compounds **3g**, **3r** and **3u**). The interactions of the synthesized compounds with the surrounding amino acids involved in the receptor are depicted in the structure–activity relationships as shown in Fig. 8.

## Conclusions

The compounds were designed and synthesized that exhibited better drug acceptance property (see supplementary material) and showed the same binding interactions as that of triclosan (Tyr158 and $NAD^+$) with additional aldehydic interaction (Met98) to enoyl-ACP receptor. Our main objective here was to develop drug-liking molecules that are better to fit into a receptor, such that one can prevail over the resistance that is due to a decrease in volume of enoyl-ACP enzyme, and from total volume, total surface area from the Crash score and steric counter map analysis, we can firmly presume that the pharmacophores designed in this study are better fit to enoyl-ACP reductase. The 3D-QSAR studies, CoMFA and CoMSIA models showed the high correlative and predictive power. A high bootstrapped $r^2$ value along with a small standard deviation indicated that a similar relationship exists in all the compounds. From our work, it can be speculated that the hit molecule **3k** can serve as a better candidate, which can be easily fit into the mutant enoyl-ACP reductase enzyme. Due to aldehydic group on pyrrole, compound **3f** is able to generate an extra interaction with the enzyme, while other molecules retain the usual interactions as that of TCL.

**Acknowledgments** Authors immensely thank research support from the Board of Research in Nuclear Sciences (BRNS), Bhabha Atomic Research Centre (BARC), Mumbai (File No. 2013/37B/17/BRNS/0417 dated-14/05/2013). We also thank Dr. V. H. Kulkarni, Principal and Mr. H. V. Dambal, President, S.E.T's College of Pharmacy, Dharwad, India for providing the facilities. The authors are grateful to Mr. Ravindra N. Nadagir and Mr. Shrikant A. Tiwari for their technical assistance.

## References

Agarwal A, Pearson PP, Taylor EW, Li HB, Dahlgren T, Herslof M, Yang Y, Lambert G, David L (1993) Three-dimensional quantitative structure–activity relationships of 5-HT receptor binding data for tetrahydropyridinylindole derivatives: a comparison of the Hansch and CoMFA methods. J Med Chem 36:4006–4014

Baldock C, Rafferty JB, Sedelnikova SE, Baker PJ, Stuitje AR, Slabas AR, Hawkes TR, Rice DW (1996) A mechanism of drug action revealed by structural studies of enoyl reductase. Science 274:2107–2110

Banerjee A, Dubnau E, Quemard A, Balasubramanian V, Um KS, Wilson T, Collins D, de-Lisle G, Jacobs WR Jr (1994) InhA, a gene encoding a target for isoniazid and ethionamide in *Mycobacterium tuberculosis*. Science 263:227–230

Biava M, Fioravanti R, Porretta GC, Sleiter G, Ettorre A, Deidda D, Lampis G, Pompei R (1997) New toluidine derivatives with antimycobacterial and antifungal activities. Med Chem Res 7:228–250

Bush BL, Nachbar RB (1993) Sample-distance partial least squares: PLS optimized for many variables, with application to CoMFA. J Comput Aided Mol Des 7:587–619

Chhibber M, Kumar G, Parasuraman P, Ramya TN, Surolia N, Surolia A (2006) Novel diphenyl ethers: design, docking studies, synthesis and inhibition of enoyl-ACP reductase of *Plasmodium falciparum* and *Escherichia coli*. Bioorg Med Chem 14:8086–8098

Chin WW (1998) The partial least squares approach to structural equation modeling. In: Marcoulides GA (ed) Modern methods for business research. Lawrence Erlbaum Associates, Mahwah, NJ, pp 295–336

Clark M, Richard D, Cramer RD III, Opdenbosch NV (1989) Validation of the general purpose tripos 5.2 force field. J Comput Chem 10:982–1012

Clark M, Cramer RD III, Jones DM, Patterson DE, Simeroth PE (1990) Comparative molecular field analysis (CoMFA) 2. Toward its use with 3D-structural databases. Tetrahedron Comp Methodol 3:47–59

Clark RD, Strizhev A, Leonard JM, Blake JF, Matthew JB (2002) Consensus scoring for ligand/protein interactions. J Mol Graph Model 20:281–295

Cramer RD III, Bunce JD, Patterson DE, Frank IE (1988) Cross validation, bootstrapping, and partial least squares compared with multiple regression in conventional QSAR studies. Mol Inf 7:18–25

Cramer RD III, Patterson DE, Bunce JD (1989) Recent advances in comparative molecular field analysis (CoMFA). Prog Clin Biol Res 291:161–165

Deidda D, Lampis G, Fioravanti R, Biava M, Porretta GC, Zanetti S, Pompei R (1998) Bactericidal activities of the pyrrole derivative BM212 against multidrug-resistant and intramacrophagic *Mycobacterium tuberculosis* strains. Antimicrob Agents Chemother 42:3035–3037

Eldridge MD, Murray CW, Auton TR, Paolini GV, Mee RP (1997) Empirical scoring functions: I. The development of a fast empirical scoring function to estimate the binding affinity of ligands in receptor complexes. J Comput Aided Mol Des 11:425–445

Espinal MA, Laszlo A, Simonsen L, Boulahbal F, Kim SJ, Reniero A, Hoffner S, Rieder HL, Binkin N, Dye C, Williams R, Raviglione MC (2001) Global trends in resistance to antituberculosis drugs. N Engl J Med 344:1294–1303

Faustini A, Hall AJ, Perucci CA (2006) Risk factors for multidrug resistant tuberculosis in Europe: a systematic review. Thorax 61:158–163

Fioravanti R, Biava M, Porretta GC, Artico M, Lampis G, Deidda D, Pompei R (1997) *N*-substituted 1-aryl-2(1*H*-imidazol-1-yl)1-ethanamines with broad spectrum in vitro antimycobacterial and antifungal activities. Med Chem Res 7:87–97

Fischer F, Matthisson M, Herrling P (2004) List of drugs in development for neurodegenerative diseases. Neurodegener Dis 1:50–70

Franzblau SG, Witzig RS, McLaughlin JC, Torres P, Madico G, Hernandez A, Degnan MT, Cook MB, Quenzer VK, Ferguson RM, Gilman RH (1998) Rapid, low-technology MIC determination with clinical *Mycobacterium tuberculosis* isolates by using the Microplate Alamar Blue Assay. J Clin Microbiol 3:362–366

Heath RJ, Rock CO (1995) Enoyl-acyl carrier protein reductase (FabI) plays a determinant role in completing cycles of fatty acid elongation in *Escherichia coli*. J Biol Chem 270:26538–26542

Heath RJ, Li J, Roland GE, Rock CO (2000) Inhibition of the *Staphylococcus aureus* NADPH-dependent enoyl-acyl carrier protein reductase by triclosan and hexachlorophene. J Biol Chem 275:4654–4659

Johnsson K, Schultz PG (1994) Mechanistic studies of the oxidation of isoniazid by the catalase peroxidase from *Mycobacterium tuberculosis*. J Am Chem Soc 116:7425–7426

Johnsson K, King DS, Schultz PG (1995) Studies on the mechanism of action of isoniazid and ethionamide in the chemotherapy of tuberculosis. J Am Chem Soc 117:5009–5010

Jones G, Willett P, Glen RC, Leach AR, Taylor R (1997) Development and validation of a genetic algorithm for flexible docking. J Mol Biol 267:727–748

Joshi SD, Vagdevi HM, Vaidya VP, Gadaginamath GS (2008) Synthesis of new 4-pyrrol-1-yl benzoic acid hydrazide analogs and some derived oxadiazole, triazole and pyrrole ring systems, a novel class of potential antibacterial and antitubercular agents. Eur J Med Chem 43:1989–1996

Joshi SD, More UA, Kulkarni VH (2013a) Synthesis, antimicrobial and cytotoxic activity of new heterocyclic hybrids based on 2,5-dimethylpyrrole and pyrrole scaffolds. Indian J Pharm Sci 75:310–323

Joshi SD, More UA, Pansuriya K, Aminabhavi TM, Gadad AK (2013b) Synthesis and molecular modeling studies of novel pyrrole analogs as antimycobacterial agents. J Saudi Chem Soc. doi:10.1016/j.jscs.2013.09.002

Joshi SD, More UA, Aminabhavi TM, Badiger AM (2014a) Two- and three-dimensional QSAR studies on a set of antimycobacterial pyrroles: CoMFA, Topomer CoMFA, and HQSAR. Med Chem Res 23:107–126

Joshi SD, More UA, Dixit SR, Korat HH, Aminabhavi TM, Badiger AM (2014b) Synthesis, characterization, biological activity, and 3D-QSAR studies on some novel class of pyrrole derivatives as antitubercular agents. Med Chem Res 23:1123–1147

Kitagawa H, Kumura K, Takahata S, Iida M, Atsumi K (2007) 4-Pyridone derivatives as new inhibitors of bacterial enoyl-ACP reductase FabI. Bioorg Med Chem 15:1106–1116

Kuntz ID, Blaney JM, Oatley SJ, Langridge R, Ferrin TE (1982) A geometric approach to macromolecule–ligand interactions. J Mol Biol 161:269–288

La Rosa V, Poce G, Canseco JO, Buroni S, Pasca MR, Biava M, Raju RM, Porretta GC, Alfonso S, Battilocchio C, Javid B, Sorrentino F, Loerger TR, Sacchettinic JC, Manetti F, Botta M, Logu AD, Rubin EJ, Rossi ED (2012) MmpL3 is the cellular target of the antitubercular pyrrole derivative BM212. Antimicrob Agents Chemother 56:324–331

Levy CW, Roujeinikova A, Sedelnikova S, Baker PJ, Stuitje AR, Slabas AR, Rice DW, Rafferty JB (1999) Molecular basis of triclosan activity. Nature 398:383–384

Lourenco MCS, de Souza MVN, Pinheiro AC, Ferreira ML, Goncalves RSB, Nogueira TCM, Peralta MA (2007) Evaluation of anti-tubercular activity of nicotinic and isoniazid analogues. ARKIVOC 15:181–191

Lu H, Tonge PJ (2008) Inhibitors of FabI, an enzyme drug target in the bacterial fatty acid biosynthesis pathway. Acc Chem Res 41:11–20

Luckner SR, Liu N, Ende CW, Tonge PJ, Kisker C (2010) A slow, tight binding inhibitor of InhA, the enoyl-acyl carrier protein reductase from *Mycobacterium tuberculosis*. J Biol Chem 285:14330–14337

Mallegol T, Gmouh S, Meziane MAA, Desce MB, Mongin O (2005) Practical and efficient synthesis of tris(4-formylphenyl)amine, a key building block in materials chemistry. Synthesis 11:1771–1774

McMurry LM, Oethinger M, Levy SB (1998) Triclosan targets lipid synthesis. Nature 394:531–532

More UA, Joshi SD, Aminabhavi TM, Gadad AK, Mallikarjuna NN, Kulkarni VH (2014) Design, synthesis, molecular docking and 3D-QSAR studies of potent inhibitors of enoyl-acyl carrier protein reductase as potential antimycobacterial agents. Eur J Med Chem 71:199–218

Muegge I, Martin YC (1999) A general and fast scoring function for protein–ligand interactions: a simplified potential approach. J Med Chem 42:791–804

Park HS, Yoon YM, Jung SJ, Kim CM, Kim JM, Kwak JH (2007) Antistaphylococcal activities of CG400549, a new bacterial enoyl-acyl carrier protein reductase (FabI) inhibitor. J Antimicrob Chemother 60:568–574

Quemard A, Lacave C, Laneelle G (1991) Isoniazid inhibition of mycolic acid synthesis by cell extracts of sensitive and resistant strains of *Mycobacterium aurum*. Antimicrob Agents Chemother 35:1035–1039

Quemard A, Sacchettini JC, Dessen A, Vilcheze C, Bittma R, Jacobs WR Jr, Blanchard JS (1995) Enzymatic characterization of the target for isoniazid in *Mycobacterium tuberculosis*. Biochemistry 34:8235–8241

Raviglione M, Marais B, Floyd K, Lönnroth K, Getahun H, Migliori GB, Harries AD, Nunn P, Lienhardt C, Graham S, Chakaya J, Weyer K, Cole S, Kaufmann SHE, Zumla A (2012) Scaling up interventions to achieve global tuberculosis control: progress and new developments. Lancet 379:1902–1913

Seefeld MA, Miller WH, Kenneth AN, Burgess WJ, DeWolf WE Jr, Elkins PA, Head MS, Jakas DR, Janson CA, Keller PM, Manley PJ, Moore TD, Payne DJ, Pearson S, Polizzi BJ, Qiu X, Rittenhouse SF, Uzinskas IN, Wallis NG, Huffman WF (2003) Indole naphthyridinones as inhibitors of bacterial enoyl-ACP reductases FabI and FabK. J Med Chem 46:1627–1635

Sivaraman S, Sullivan TJ, Johnson F, Novichenok P, Cui G, Simmerling C, Tonge PJ (2004) Inhibition of the bacterial enoyl reductase FabI by triclosan: a structure–reactivity analysis of FabI inhibition by triclosan analogues. J Med Chem 47:509–518

Sullivan TJ, Truglio JJ, Boyne ME, Novichenok P, Zhang X, Stratton CF, Li HJ, Kaur T, Amin A, Johnson F, Slayden RA, Kisker C, Tonge PJ (2006) High affinity InhA inhibitors with activity against drug-resistant strains of *Mycobacterium tuberculosis*. ACS Chem Biol 1:43–53

Thomas G (2007) Structure–activity and quantitative structure relationships. medicinal chemistry an introduction, 2nd edn. Wiley, New York, pp 75–110

Tipparaju SK, Mulhearn DC, Klein GM, Chen Y, Tapadar S, Bishop MH, Yang S, Chen J, Ghassemi M, Santarsiero BD, Cook JL, Johlfs M, Mesecar AD, Johnson ME, Kozikowski AP (2008) Design and synthesis of aryl ether inhibitors of the *Bacillus anthracis* enoyl-ACP reductase. Chem Med Chem 3:1250–1268

Tripos International (2012) Sybyl-X 2.1.1, Tripos International, St. Louis, MO, USA

Varela C, Rittmann D, Singh A, Krumbach K, Bhatt K, Eggeling L, Besra GS, Bhatt A (2012) MmpL genes are associated with mycolic acid metabolism in mycobacteria and Corynebacteria. Chem Biol 19:498–506

Vilsmeier A, Haack A (1927) Uber die einwirkung von halogen-phosphor auf alkyl-formanilide. eine neue methode zur darstellung sekundarer und tertiarer *p*-alkylamino-benzaldehyde. Eur J Inorg Chem 60:119–122

WHO (2012) Global tuberculosis report 2012. World Health Organization, Geneva, Switzerland

World Health Organization (WHO) (2010) Multidrug and extensively drug-resistant TB (M/XDR-TB). (2010) Global report on surveillance and response. WHO/HTM/TB/2010.3. Geneva, Switzerland. http://whqlibdoc.who.int/publications/2010/9789241599191_eng.pdf

Zhang Y, Heym B, Allen B, Young D, Cole S (1992) The catalase–peroxidase gene and isoniazid resistance of *Mycobacterium tuberculosis*. Nature 358:591–593